NAVAL POSTGRADUATE SCHOOL

MONTEREY, CALIFORNIA

THESIS

DIGITAL COMMUNICATIONS OVER NON-FADING AND FADING CHANNELS

by

Jose H. Hernandez Jr.

September 2008

Thesis Advisor: Clark Robertson
Second Reader: Frank Kragh

Approved for public release; distribution unlimited

THIS PAGE INTENTIONALLY LEFT BLANK

REPORT DOCUMENTATION PAGE			Form Approved OMB No. 0704-0188
Public reporting burden for this collection of information is estimated to average 1 hour per response, including the time for reviewing instruction, searching existing data sources, gathering and maintaining the data needed, and completing and reviewing the collection of information. Send comments regarding this burden estimate or any other aspect of this collection of information, including suggestions for reducing this burden, to Washington headquarters Services, Directorate for Information Operations and Reports, 1215 Jefferson Davis Highway, Suite 1204, Arlington, VA 22202-4302, and to the Office of Management and Budget, Paperwork Reduction Project (0704-0188) Washington DC 20503.			
1. AGENCY USE ONLY ***(Leave blank)***	**2. REPORT DATE** September 2008	**3. REPORT TYPE AND DATES COVERED** Master's Thesis	
4. TITLE AND SUBTITLE: Digital Communications Over Non-Fading and Fading Channels			**5. FUNDING NUMBERS**
6. AUTHOR Jose H. Hernandez Jr.			
7. PERFORMING ORGANIZATION NAME(S) AND ADDRESS(ES) Naval Postgraduate School Monterey, CA 93943-5000			**8.PERFORMING ORGANIZATION REPORT NUMBER**
9. SPONSORING /MONITORING AGENCY NAME(S) AND ADDRESS(ES) N/A			**10. SPONSORING/MONITORING AGENCY REPORT NUMBER**
11. SUPPLEMENTARY NOTES The views expressed in this thesis are those of the author and do not reflect the official policy or position of the Department of Defense or the U.S. Government.			
12a. DISTRIBUTION / AVAILABILITY STATEMENT Approved for public release; distribution unlimited			**12b. DISTRIBUTION CODE** A

13. ABSTRACT (maximum 200 words)

The objective of this thesis is to enhance the ability of the Improved Many-on-Many (IMOM) software package to analyze modern digital communication systems using available intelligence. Currently, IMOM can only be used to analyze analog communication systems, but modern systems are, increasingly digital. In this thesis, the probability of bit error expressions for many common digital modulation techniques, both binary and non-binary, are inverted to obtain expressions for the required signal-to-noise ratio as a function of probability of channel bit error. Furthermore, results are obtained not only for a non-fading channel but for channels modeled as either Rayleigh or Ricean. These equations can be implemented in IMOM to increase the accuracy of the link budget analysis when the specific modulation type being evaluated is known. This thesis takes the approach of determining probability of channel bit error rather than information bit error, which allows generic solutions independent of the specifics of the system under investigation as long as the particular modulation type is known. When even greater accuracy is desired, system specifics such as the type of error control coding must be taken into account. As an example of this, the Joint Tactical Information Distribution System (JTIDS) is considered.

14. SUBJECT TERMS coherent, noncoherent, BPSK, QPSK, MPSK, MQAM, GMSK, MFSK, JTIDS, multipath, signal fading, IMOM			**15. NUMBER OF PAGES** 95
			16. PRICE CODE
17. SECURITY CLASSIFICATION OF REPORT Unclassified	**18. SECURITY CLASSIFICATION OF THIS PAGE** Unclassified	**19. SECURITY CLASSIFICATION OF ABSTRACT** Unclassified	**20. LIMITATION OF ABSTRACT** UU

NSN 7540-01-280-5500 Standard Form 298 (Rev. 2-89)
Prescribed by ANSI Std. 239-18

THIS PAGE INTENTIONALLY LEFT BLANK

Approved for public release; distribution unlimited

DIGITAL COMMUNICATIONS OVER NON-FADING AND FADING CHANNELS

Jose H. Hernandez Jr.
Captain, United States Marine Corps
BS Industrial Engineering, Texas A&M University, 2001

Submitted in partial fulfillment of the
requirements for the degree of

MASTER OF SCIENCE IN ELECTRICAL ENGINEERING

from the

NAVAL POSTGRADUATE SCHOOL
September 2008

Author: Jose H. Hernandez Jr.

Approved by: R. Clark Robertson
Thesis Advisor

Frank Kragh
Second Reader

Jeffrey B. Knorr
Chairman, Department of Electrical and Computer Engineering

THIS PAGE INTENTIONALLY LEFT BLANK

ABSTRACT

The objective of this thesis is to enhance the ability of the Improved Many-on-Many (IMOM) software package to analyze modern digital communication systems using available intelligence. Currently, IMOM can only be used to analyze analog communication systems, but modern systems are, increasingly, digital. In this thesis, the probability of bit error expressions for many common digital modulation techniques, both binary and non-binary, are inverted to obtain expressions for the required signal-to-noise ratio as a function of probability of channel bit error. Furthermore, results are obtained not only for a non-fading channel but for channels modeled as either Rayleigh or Ricean. These equations can be implemented in IMOM to increase the accuracy of the link budget analysis when the specific modulation type being evaluated is known. This thesis takes the approach of determining probability of channel bit error rather than information bit error, which allows generic solutions independent of the specifics of the system under investigation as long as the particular modulation type is known. When even greater accuracy is desired, system specifics such as the type of error control coding must be taken into account. As an example of this, the Joint Tactical Information Distribution System (JTIDS) is considered.

THIS PAGE INTENTIONALLY LEFT BLANK

TABLE OF CONTENTS

LIST OF FIGURES

LIST OF TABLES

THIS PAGE INTENTIONALLY LEFT BLANK

EXECUTIVE SUMMARY

The 453rd Electronic Warfare Squadron is the leading authority in improving the Improved-Many-On-Many (IMOM) modeling tool for the United States Air Force. IMOM is a two-dimensional, graphical-oriented, radio frequency modeling tool used for mission and planning intelligence. In an effort to improve the product, the effects of digital modulation techniques must be included in the system. Currently, only analog modulation schemes are incorporated into the architecture.

The objective of this thesis is to enhance the ability of the Improved Many-on-Many (IMOM) software package to analyze modern digital communication systems using available intelligence. Currently, IMOM can only be used to analyze analog communication systems, but modern systems are, increasingly, digital. In this thesis, the probability of bit error expressions for many common digital modulation techniques, both binary and non-binary, are inverted to obtain expressions for the required signal-to-noise ratio as a function of probability of channel bit error. Furthermore, results are obtained not only for a non-fading channel but for channels modeled as either Rayleigh or Ricean. The probability of channel bit error equations for coherently detected binary phase-shift keying (BPSK), quadrature phase-shift keying (QPSK), *M*-ary phase-shift keying (*M*PSK), *M*-ary quadrature amplitude modulation (*M*QAM), and Gaussian minimum-shift keying (GMSK) and noncoherently detected *M*-ary frequency-shift keying (MFSK) are inverted, in some cases numerically, and, in the case of fading channels, numerically using logarithmic regression techniques.

These equations can be implemented in IMOM to increase the accuracy of the link budget analysis when the specific modulation type being evaluated is known. This thesis takes the approach of determining probability of channel bit error rather than information bit error, which allows generic solutions independent of the specifics of the system under investigation as long as the particular modulation type is known. When even greater accuracy is desired, system specifics such as the type of error control coding must be taken into account. As an example of this, the Joint Tactical Information Distribution System (JTIDS) is considered.

THIS PAGE INTENTIONALLY LEFT BLANK

ACKNOWLEDGMENTS

I dedicate this work to my loving wife Janene, and three great sons Noah, Elijah and Jeremiah. Their support and dedication have been instrumental, not only to this thesis, but to my military career.

I would also like to give my sincere appreciation to Professor Clark Robertson for his support and confidence in me while at the Naval Postgraduate School.

THIS PAGE INTENTIONALLY LEFT BLANK

I. INTRODUCTION

A. OVERVIEW

Improved many-on-many (IMOM) is a two-dimensional, graphical-oriented, radio frequency modeling tool used for mission and planning intelligence. The tool can be used for electronic attack, electronic support, command and control, communications, computers and intelligence (C4I) and for mission planning and intelligence. *Many-on-many* refers to many targets versus many collectors/jammers, while *improved* reflects an aspiring dedication to continually advance the product. Current IMOM calculations are based on various analog modulations. The goal of the U.S. Air Force and, specifically, the 453rd Electronic Warfare Squadron (EWS) is to incorporate digital modulation waveforms into IMOM. In order to do so, reverse engineering of previously analyzed digital communications signals needs to be modified for easy incorporation into the link budget analysis equation [1], Equation Section 1

$$M_{dB} = EIRP_{dBW} + G_{r\,dBi} - T_{S_{dBK}} - L_{C_{dB}} - L_{0_{dB}} - R_{b_{dB-Hz}} - \left(\frac{E_b}{N_0}\right)_{\min_{dB}} + 228.6_{dBW/K-Hz} \quad (1.1)$$

where M_{dB} is the link margin expressed in decibels, $EIRP_{dBW}$ is the effective isotropic radiated power, $G_{r\,dBi}$ is the gain of the receiving antenna, $T_{S_{dBK}}$ is the system equivalent noise temperature, $L_{C_{dB}}$ is the free space channel loss, $L_{0_{dB}}$ represents miscellaneous losses not accounted for, $R_{b_{dB-Hz}}$ is the data rate of the signal, $\left(E_b/N_0\right)_{\min_{dB}}$ is the minimum signal-to-noise ratio required to close the link, and $-228.6_{dBW/K-Hz}$ represents Boltzmann's constant.

The term $\left(E_b/N_o\right)_{\min_{dB}}$ is the minimum allowed signal-to-noise ratio at the receiver which satisfies the probability of bit error specification of the system under consideration and accounts for the small scale fading losses of the communications link.

In order to implement Equation (1.1) directly, systems are typically evaluated to obtain the probability of channel error as a function of the signal-to-noise ratio.

B. THESIS OBJECTIVE

The primary objective of this thesis is to invert probability of bit error equations for common digital communications modulation formats and determine the range of applicability of the inverted equations. The equations are intended for implementation in the IMOM architecture. Currently, the architecture does not take into account digital modulation techniques, making it imprecise for applications where digital communications are used. The probability of channel bit error equations for coherently detected binary phase-shift keying (BPSK), quadrature phase-shift keying (QPSK), *M*-ary phase-shift keying (*M*PSK), *M*-ary quadrature phase-shift keying (*M*QAM), and Gaussian minimum-shift keying (GMSK) and noncoherently detected *M*-ary frequency-shift keying (MFSK) are inverted, in some cases numerically, and, in the case of Ricean fading channels, numerically using logarithmic regression techniques. To the best of the author's knowledge, this is the first time, except for the simplest cases such as noncoherent binary FSK (BFSK), that a comprehensive catalog of inverted probability of bit error equations for all the major modulation types, including the effects of small-scale fading, has been done. Furthermore, this thesis takes the novel approach of determining probability of channel bit error rather than information bit error, which allows generic solutions independent of the specifics of the system under investigation as long as the particular modulation type is known. Finally, as an example of a specific system, the Joint Tactical Information Distribution System (JTIDS) is evaluated to determine $\left(E_b/N_0\right)_{\min_{dB}}$ for the first time in this thesis.

C. THESIS OUTLINE

This thesis is organized into seven chapters, including the introductory material in this chapter. Insight into the background of the derivations obtained throughout this thesis, are given in Chapter II. The probability channel bit error equations for coherent BPSK, QPSK, *M*PSK, *M*QAM and GMSK and noncoherent *M*FSK in additive white

Gaussian noise (AWGN) for nonfading, Rayleigh and Ricean fading communications channels are inverted in Chapters III, IV and V, respectively. The methodology is applied to JTIDS in Chapter VI. A culmination of the previous chapters and the results and the conclusion of the thesis are given in Chapter VII.

THIS PAGE INTENTIONALLY LEFT BLANK

II. BACKGROUND

The modulation techniques evaluated in this thesis are among the most common types of digital modulation schemes available for wireless communications and military applications. They are utilized in both U.S. and European wireless communication standards and in aerospace applications in the Armed Forces. The approach taken in the majority of this thesis is not meant to be all inclusive but to provide a generic methodology that can be implemented regardless of the system being evaluated as long as the specific modulation technique is known.

The coherent modulation techniques BPSK, QPSK, *M*PSK, *M*QAM and GMSK are evaluated for a non-fading, a Rayleigh fading and a Ricean fading channel. In addition a common non-coherent modulation technique, *M*FSK is evaluated for the same channel types. The equations used to evaluate the performance of the various modulation techniques are obtained from published literature.Equation Chapter (Next) Section 2

A. GENERIC, SYSTEM INDEPENDENT APPROACH

Forward error correction (FEC) coding significantly improves the performance of communications systems. The calculations and formulas derived for this project assume that error control coding has been implemented. The equations are intended to be generic in nature to remain flexible enough to adapt to different code rates and different code types as dictated by a specific system. The two primary types of FEC codes are block codes and convolutional codes. Only the performance of JTIDS is calculated precisely. The intent of using JTIDS as an example, in addition to the obvious interest in this particular system, is to show the capability that exists when specific system details are known. The generic equations can easily be tailored to specific systems if the system details, such as type of FEC coding used, are known.

In order to understand the generic approach that depends only on the probability of channel bit error, it is important to understand the demodulation process. The

probability of channel bit error is a figure of merit related to the demodulation process and is a measure of the quality of the demodulated bits entering the channel decoder as shown in Figure 1.

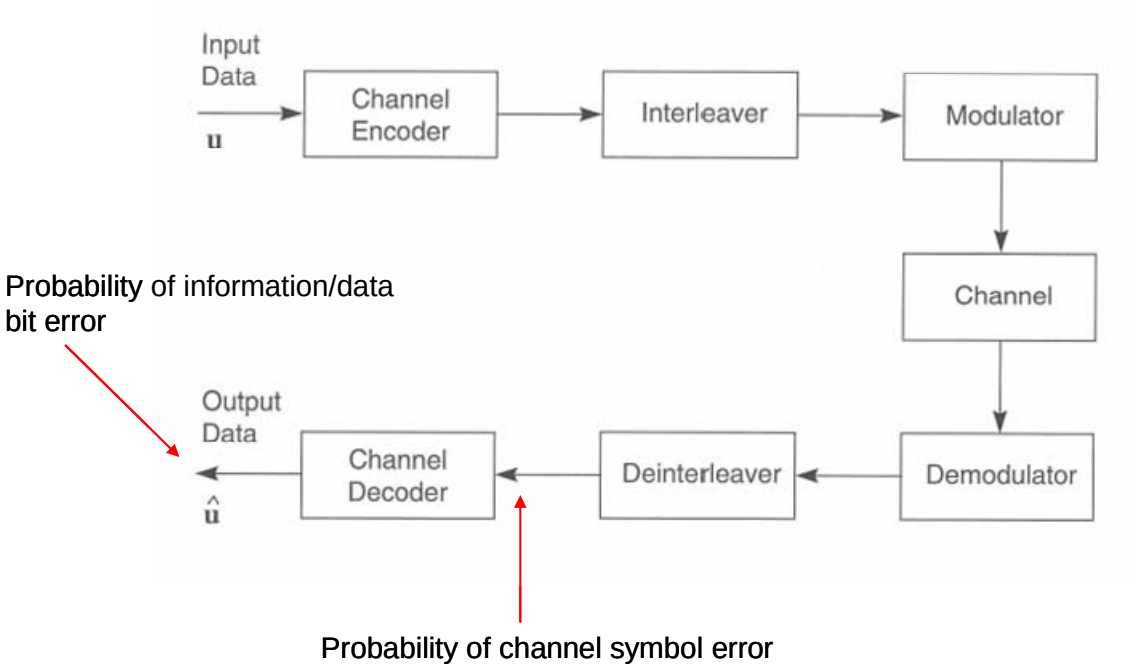

Figure 1. Information bit error and channel bit error relationship [4].

The probability of channel bit error, prior to the channel decoder, directly impacts the output, or information, bit error. Since the specifics of some systems may be unknown, it is necessary to determine a range of probability of channel bit error that will be valid for most applications. Since wireless communications systems are often specified for a probability of information bit error of 10^{-5}, and since all modern digital communication systems use FEC codes, a generic range was determined [6]. For example, using the performance of systems with convolutional coding and hard decision decoding for various commonly used code rates, the relationship between information bit error P_b and the probability of channel bit error, p, is shown in Figure 2. We see that the range $0.0055 \le p \le 0.055$ corresponds to $10^{-6} \le P_b \le 10^{-4}$.

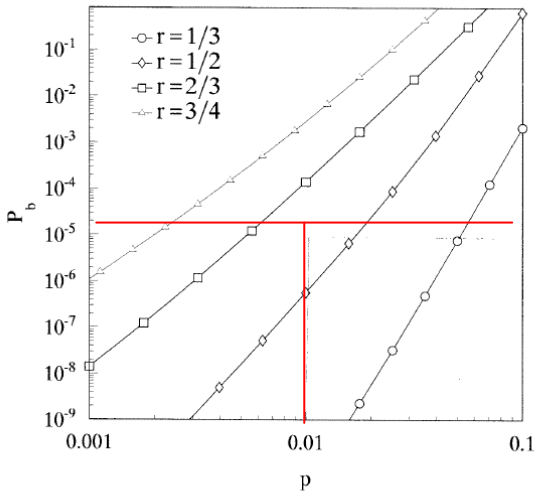

Performance of systems with $K = 6$ convolutional source coding and hard decision decoding.

Figure 2. Probability of channel bit error vs. information bit error [4].

As can be seen from Figure 2, a probability of channel bit error $p = 10^{-2}$ is more or less in the middle of the range of p values that yield a probability of information bit error of $P_b = 10^{-5}$. In the remainder of this thesis, p_b is used to represent the probability of channel bit error instead of p as in Figure 2.

B. COHERENT MODULATION TECHNIQUES

A precise equation for probability of channel bit error for the coherent modulation techniques considered in this thesis is given by [2]

$$p_b = \frac{a}{q} Q\left(\sqrt{bq\gamma_b}\right) \tag{2.1}$$

where $\gamma_b = E_b / N_o$ is the average energy per bit (E_b)-to-noise power spectral density (N_o) ratio, and a specific modulation technique is defined by the modulation dependent parameters a, q and b [2]. These parameters are shown in Table 1. Note that for *M*QAM there is a difference for even and odd values of q. Even values for q such as 16-QAM and 64-QAM are more commonly used in applications such as in wireless communication standards.

Table 1. Modulation Dependent Constants.

Modulation	*q*	*a*	*b*
BPSK	1	1	2
QPSK	2	2	1
MPSK	$\log_2 M$	2	$2\sin^2(\pi/M)$
MQAM	4,6,…	$4(1-2^{-q/2})$	$3/(2^q - 1)$
MQAM	3,5,…	4	$3/(2^q - 1)$
GMSK	1	1	2δ

In order to use the approximate equations for the coherent modulation techniques, it was necessary to ensure that the approximate equations presented a good representation of the exact equations for the scheme being used. In order to establish this relationship, an example for BPSK is used.

Equation (2.1) can be approximated by [2]

$$p_b \approx \frac{a}{q}\left(\frac{1}{\sqrt{2\pi bq\gamma_{b\min}}}\right)\exp\left(-\frac{1}{2}bq\gamma_b\right), \tag{2.2}$$

which incorporates a slightly modified version of a common approximation for the Q-function. Specifically, γ_b in the radical has been replaced with $\gamma_{b\min}$, a constant that is determined for each of the coherent modulation techniques discussed in order to optimize the results over a range of p_b as previously discussed.

The results from plotting Equations (2.1) and (2.2) for BPSK are shown in Figure 3. The $\gamma_{b\min}$ used for BPSK was optimized for the region of interest for BPSK and centered around $p_b = 10^{-2}$. In this case $\gamma_{b\min} = 2.5\,\text{dB}$ was used and resulted in a nearly identical approximation for the range of values being considered. The other coherent modulation techniques considered are tested using the same method and yield similar results. Variations between the actual results and approximate results differ at most by 0.5 dB over the range of interest, and for BPSK differ by at most 0.3 dB. These values are small enough to be considered negligible for the purpose of this project and for incorporation into IMOM.

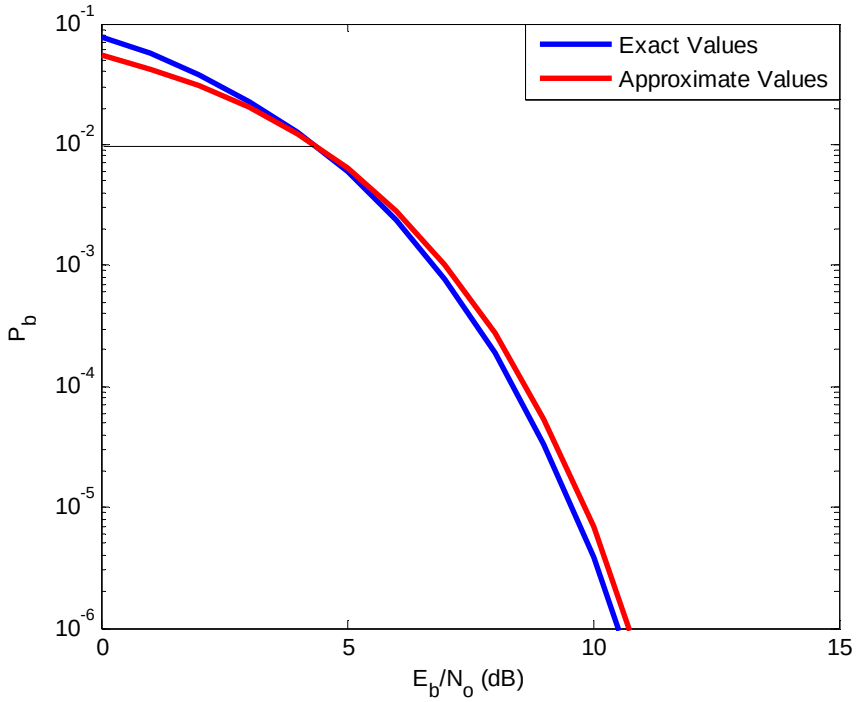

Figure 3. BPSK performance in AWGN (comparison between exact and approximate results).

C. NONCOHERENT, ORTHOGONAL MODULATION TECHNIQUES

M-ary orthogonal signaling is considered using a similar procedure as that used for coherent modulation. The probability of channel bit error for orthogonal signaling with noncoherent detection, including orthogonal *M*FSK, is given by [2]

$$p_b = \frac{M}{2(M-1)} \sum_{n=1}^{M-1} \frac{(-1)^{n+1}}{n+1} \binom{M-1}{n} \exp\left[\frac{-nq\gamma_b}{n+1}\right] \tag{2.3}$$

where $M = 2^q$. Equation (2.3) is accurately approximated for practical applications by the first term in the summation, which corresponds to the union bound:

$$p_b \approx \frac{M}{4} \exp\left(\frac{-q\gamma_b}{2}\right). \tag{2.4}$$

D. MULTIPATH FADING CHANNELS

Many wireless communications channels do not have a line-of-sight (LOS) signal path. The lack of a LOS signal path entails transmitting a signal to the receiver by a phenomenon known as multipath. Multipath occurs when there are multiple paths from the transmitter to the receiver due to the reflection of the original signal off of buildings, terrain (features) or the ionosphere. The availability of a LOS does not necessarily mean that a multipath component does not exist. A signal that goes through a multipath fading channel will arrive at the receiver multiple times with different amplitudes, phases and arrival times. Since multipath channels can vary significantly in terms of characteristics in an unpredictable manner, they must be modeled as a random process. In addition, relative motion of the transmitter and receiver makes a multipath channel a time-varying channel. Therefore, an identical signal transmitted over the same multipath channel at a different time may exhibit different characteristics. In general, the received multipath components will add both destructively and constructively, resulting in a received signal that fluctuates in signal amplitude and phase. This is known as signal fading [3].

The most common model for a multipath fading channel is the Ricean model, where the amplitude of the received signal is modeled as a Ricean random variable. In that case, Equation (2.1) must be modified to [2]

$$p_b = \frac{a}{q}\int_0^{\infty} Q(\sqrt{bq\gamma_b})\frac{\sigma_0^2}{2\sigma^2}\exp\left[-\frac{(q\gamma_b\sigma_0^2+\alpha^2)}{2\sigma^2}\right] I_0\left(\frac{\alpha\sqrt{q\gamma_b\sigma_0^2}}{\sigma^2}\right) d\gamma_b, \qquad (2.5)$$

where I_0 is the modified Bessel function of the first kind and order zero, $2\sigma^2$ represents the non-LOS signal power, α^2 represents the LOS signal power and $\sigma_o^2 = N_o/T_s$. The one-sided power spectral density of the AWGN is N_o, and T_s is the symbol duration [4]. Generally speaking, simple inversion techniques that are used for non-fading channels do not work for Ricean fading channels due to the complexity of Equation (2.5).

E. JOINT TACTICAL INFORMATION DISTRIBUTION SYSTEM (JTIDS)

JTIDS is a network radio system used by the U.S. Armed Forces and its allies to support data communications needs. JTIDS uses (31,15) Reed Solomon (RS) coding. The modulation technique used in JTIDS is cyclical code-shift keying (CCSK), which utilizes 32 phases of a 32-chip sequence and is a quasi-orthogonal modulation scheme. JTIDS operates with both a single- and double-pulse architecture. For this thesis, the single pulse architecture was considered. The single-pulse architecture allows for greater data throughput than the double-pulse architecture. [5]

In this chapter, expressions for the channel probability of bit error for the modulation techniques considered in this thesis were provided, and a system non-specific procedure was developed to estimate the required signal-to-noise ratio given only the type of digital modulation utilized. The fundamentals necessary to account for Rayleigh and Ricean multipath fading channels were also provided. The following chapter expands on the concepts introduced in Chapter II for non-fading channels.

THIS PAGE INTENTIONALLY LEFT BLANK

III. NON-FADING CHANNELS

Non-fading channels require the minimal amount of signal power for a given modulation type and, therefore, represent a channel with only a line-of-sight signal component. While this is overly optimistic for many of today's digital communications systems, it serves as a reference when incorporating fading channels. As mentioned in the last chapter, $\gamma_b = E_b / N_0$, and γ_b is the parameter to be determined. Equation Chapter (Next) Section 3

Solving Equation (2.2) for γ_b, we get

$$\gamma_b = 10\log\left[-\frac{2}{bq}\ln\left(\frac{q\sqrt{2\pi bq\gamma_{b\min}}}{a}\right)p_b\right] \tag{3.1}$$

where

$$\gamma_{b_{\min}} = \frac{4\gamma_{b_{optimized}}}{bq}, \tag{3.2}$$

and $\gamma_{b_{optimized}}$ is obtained using trial-and-error to optimize Equation (3.1) for the range of p_b of interest.

A. COHERENT MODULATION

For BPSK and QPSK, the modulation dependent parameters listed in Table 1 have the same ratio and products and, therefore, exhibit identical performance. In the case of BPSK and QPSK, $\gamma_{b_{\min}} = 2.5$ dB, or $10^{0.25}$. Substituting $\gamma_{b_{\min}} = 2.5$ and the appropriate parameters for BPSK/QPSK from Table 1 into Equation (3.1), we get

$$\gamma_b = 10\log\left[-\ln\left(\sqrt{(4\pi\times 10^{0.25}}\right)p_b\right]. \tag{3.3}$$

A plot of Equation (3.3) is shown in Figure 4. Each graph in this thesis is marked according to the probability of channel bit error $p_b = 10^{-2}$ and the associated signal-to-noise ratio γ_b. As can be seen from Figure 4, for BPSK and QPSK $\gamma_b = 4.3$ dB is required for $p_b = 10^{-2}$.

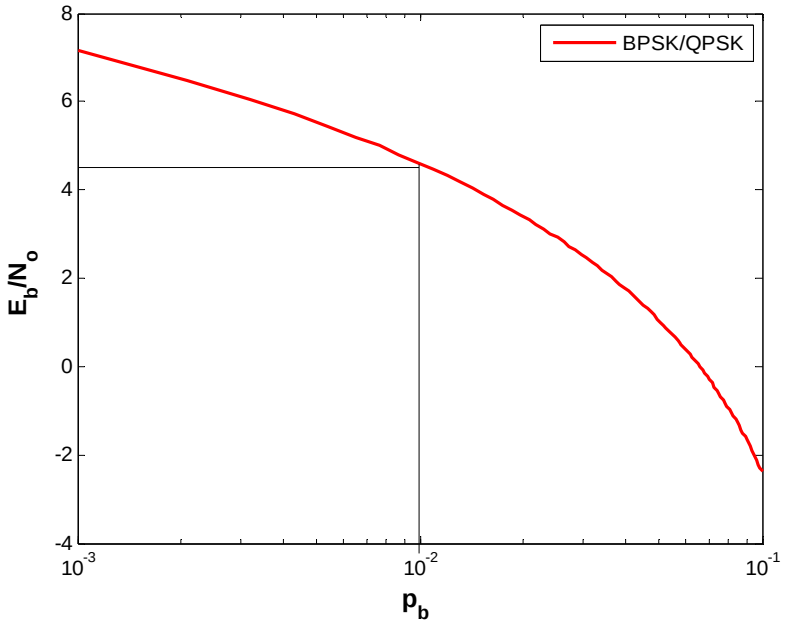

Figure 4. BPSK/QPSK performance in AWGN.

1. *M*PSK

With regard to *M*PSK, 8-PSK and 16-PSK are the most commonly used modulation schemes. *M*PSK with $M \geq 32$ is rarely used due to the excessive power required [4]. 8-PSK is used in the IEEE 802.11g wireless standard and is widely used in satellite communications [6]. As with BPSK, $\gamma_{b_{\min}} = 2.5$ dB optimizes Equation (3.1) for 8-PSK and 16-PSK. As previously mentioned, since the objective is to evaluate unknown systems, the range of probability of channel bit error of interest is $10^{-3} \leq p_b \leq 10^{-1}$. Substituting $\gamma_{b\min} = 10^{0.25}$ and the appropriate parameters from Table 1 into Equation (3.1), we obtain for 8-PSK

$$\gamma_b = 10\log\left[-\left(1.6\times10^{3}\right)\ln\left(\sqrt{\left(376\pi\times10^{-6}\right)\left(10^{0.25}\right)}\right)p_b\right], \tag{3.4}$$

and, similarly, for 16-PSK

$$\gamma_b = 10\log\left[-\left(42.6\times10^{3}\right)\ln\left(\sqrt{\left(94\pi\times10^{-6}\right)\left(10^{0.25}\right)}\right)p_b\right], \tag{3.5}$$

with the units in decibels or dB.

Plots of Equations (3.4) and (3.5) are shown in Figures 5 and 6, respectively. As can be seen, 8-PSK requires $\gamma_b = 9.7$ dB while 16-PSK requires $\gamma_b = 15.5$ dB to meet the desired probability of channel bit error $p_b = 10^{-2}$.

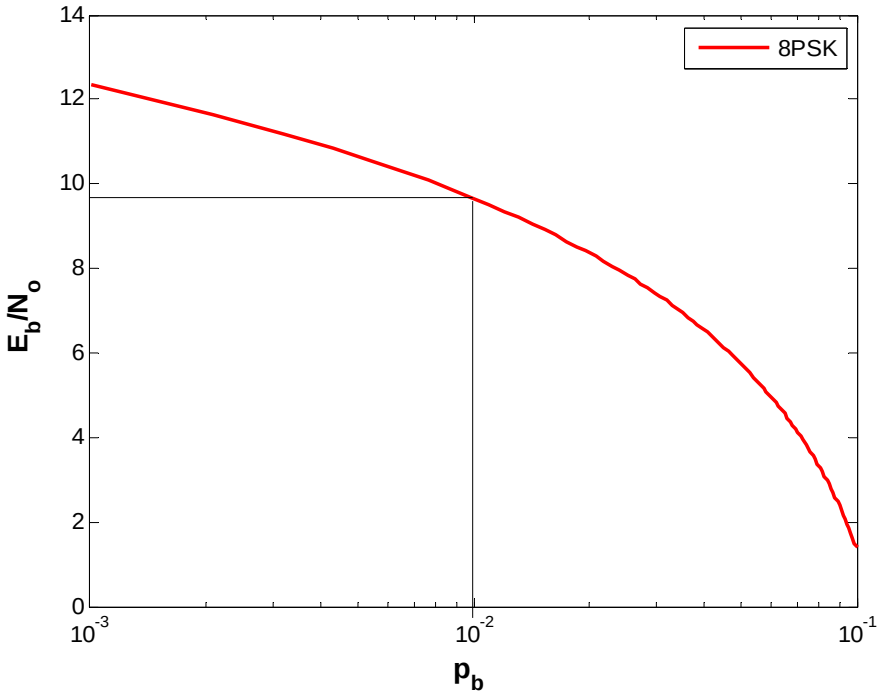

Figure 5. 8-PSK performance for a non-fading channel.

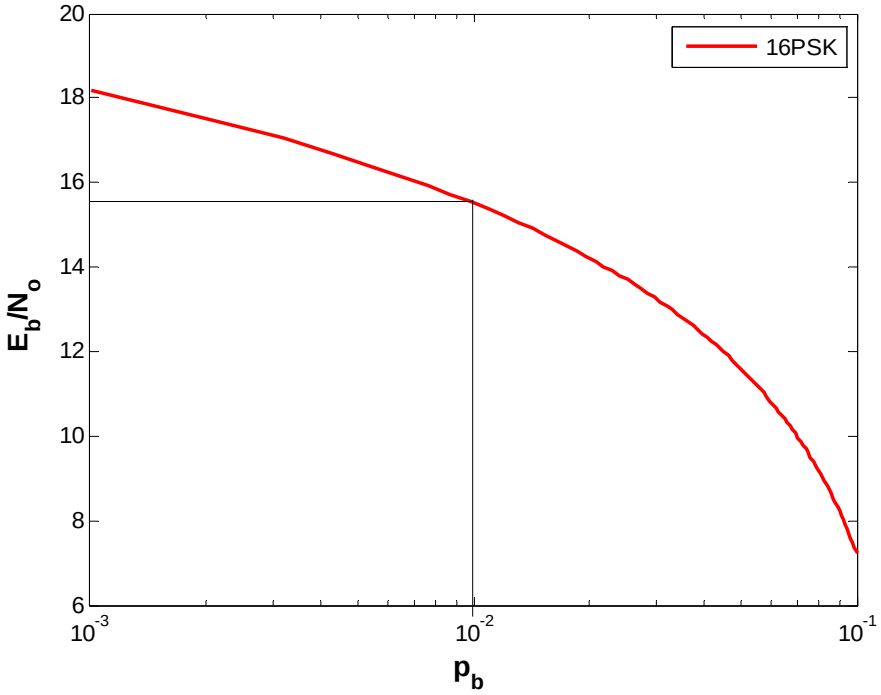

Figure 6. 16-PSK Performance for a non-fading channel.

2. *M*QAM

The analysis of *M*QAM is more complex than the previously discussed *M*PSK schemes. However, *M*QAM can be thought of as a generalization of *M*PSK where the signal constellation is not restricted to being circular. *M*QAM also differs in that different values for a, as shown in Table 1, are required for even and odd values of q. Even constellations are more common in practical applications. 16-QAM and 64-QAM are used in wireless communication standards 802.11a/g [6].

Substituting the appropriate parameters from Table 1 for 16-QAM into Equation (3.1), we get

$$\gamma_b = 10\log\left[-2.5\ln\left(3.4\sqrt{1.6\pi\times 10^{0.25}}\right)p_b\right] \tag{3.6}$$

Similarly, for 64-QAM

$$\gamma_b = 10\log\left[-6.9\ln\left(1.7\sqrt{0.576\pi\times 10^{0.25}}\right)p_b\right], \tag{3.7}$$

and for 256-QAM

$$\gamma_b = 10\log\left[-64.1\ln\left(2.1\sqrt{0.062\pi\times 10^{0.25}}\right)p_b\right] \tag{3.8}$$

where $\gamma_{b_{\min}} = 2.5$ dB is used to optimize Equations (3.6), (3.7) and (3.8) for the range of interest.

Equations (3.6), (3.7) and (3.8) are plotted in Figures 7, 8 and 9, respectively. In order to achieve $p_b = 10^{-2}$, signal-to-noise ratios of 7.8 dB, 11.8 dB and 16.2 dB are required for 16-QAM, 64-QAM and 256-QAM, respectively.

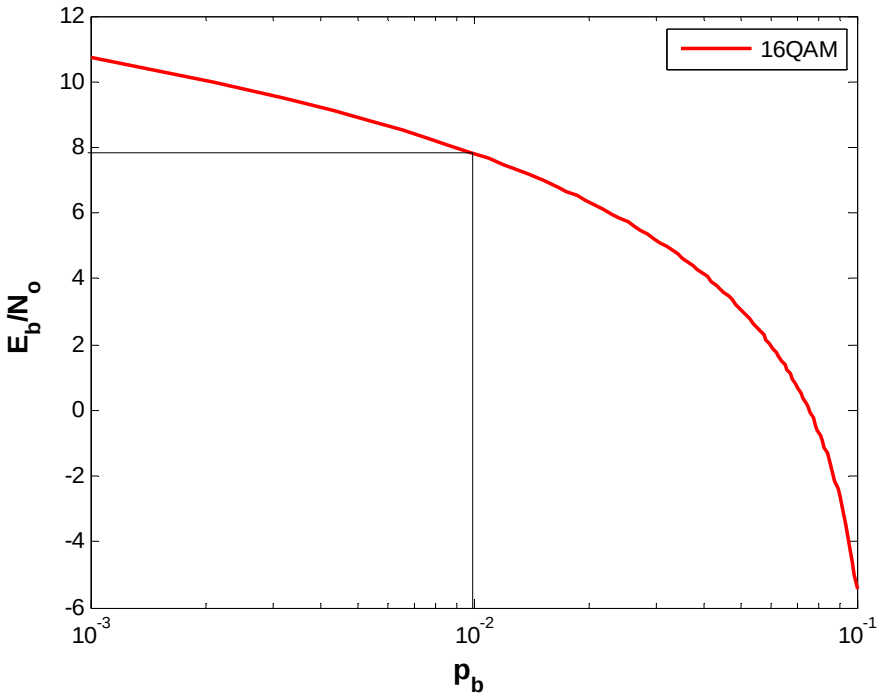

Figure 7. 16-QAM performance for a non-fading channel.

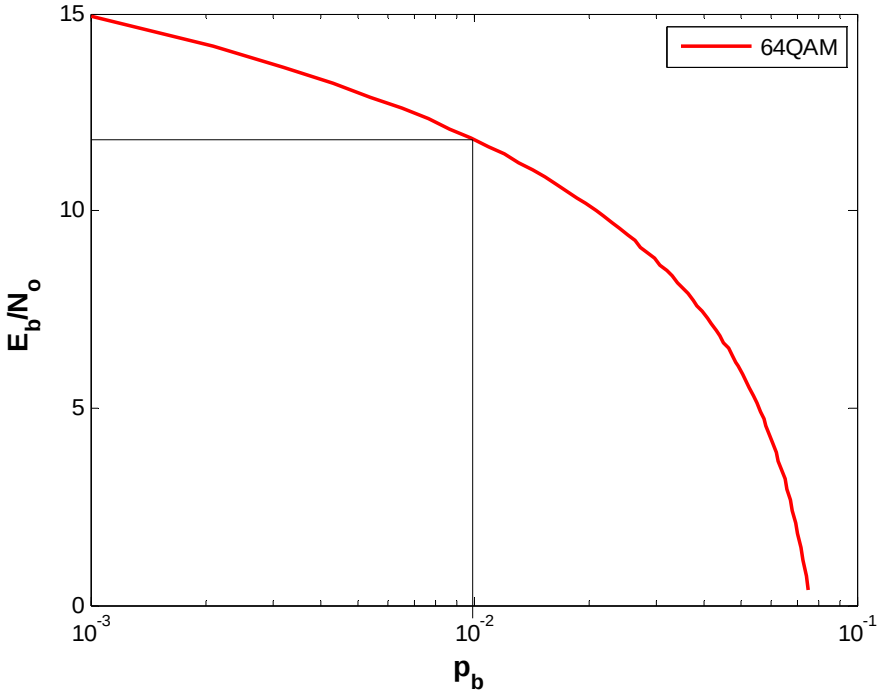

Figure 8. 64-QAM performance for a non-fading channel.

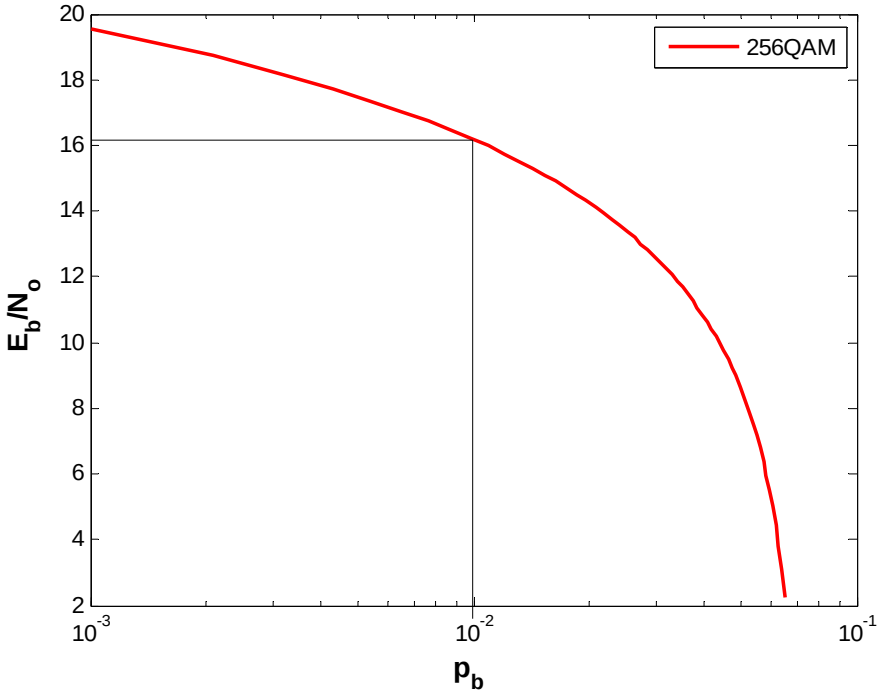

Figure 9. 256-QAM performance for a non-fading channel.

The equations developed for *M*QAM are only valid for a probability of channel bit error less than 0.065, since p_b values greater than this yield inaccurate results. This does not present any concerns since this limit is well within the desired ranges for p_b. Due to its large power consumption, 256-QAM is rarely used in wireless communications [6].

Substituting the appropriate parameters from Table 1 into Equation (3.1), for 8-QAM we get

$$\gamma_b = 10\log\left[-1.6\ln\left(0.75\sqrt{2.6\pi\times 10^{0.25}}\right)p_b\right]. \tag{3.9}$$

Similarly, for 32-QAM

$$\gamma_b = 10\log\left[-4.1\ln\left(1.25\sqrt{0.97\pi\times 10^{0.25}}\right)p_b\right], \tag{3.10}$$

and for 128-QAM,

$$\gamma_b = 10\log\left[-12.1\ln\left(1.75\sqrt{0.33\pi\times 10^{0.25}}\right)p_b\right]. \tag{3.11}$$

Equations (3.9), (3.10) and (3.11) are plotted in Figures 10, 11 and 12, respectively. As can be seen, signal-to-noise ratios of 6.7 dB, 10 dB and 14.1 dB are required for 8-QAM, 32-QAM and 128-QAM, respectively, to achieve a probability of channel bit error of 10^{-2}.

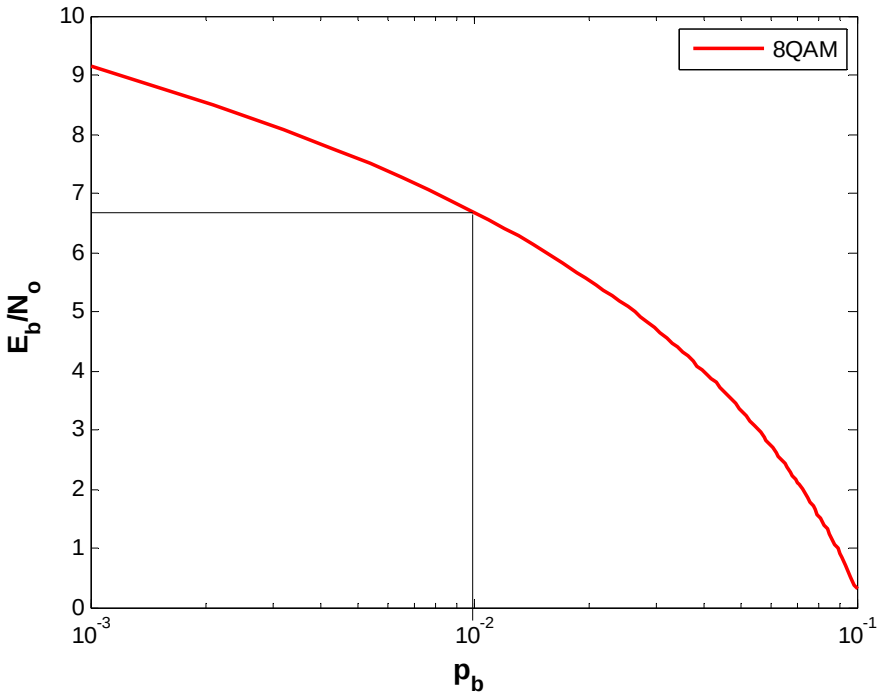

Figure 10. 8-QAM performance for a non-fading channel.

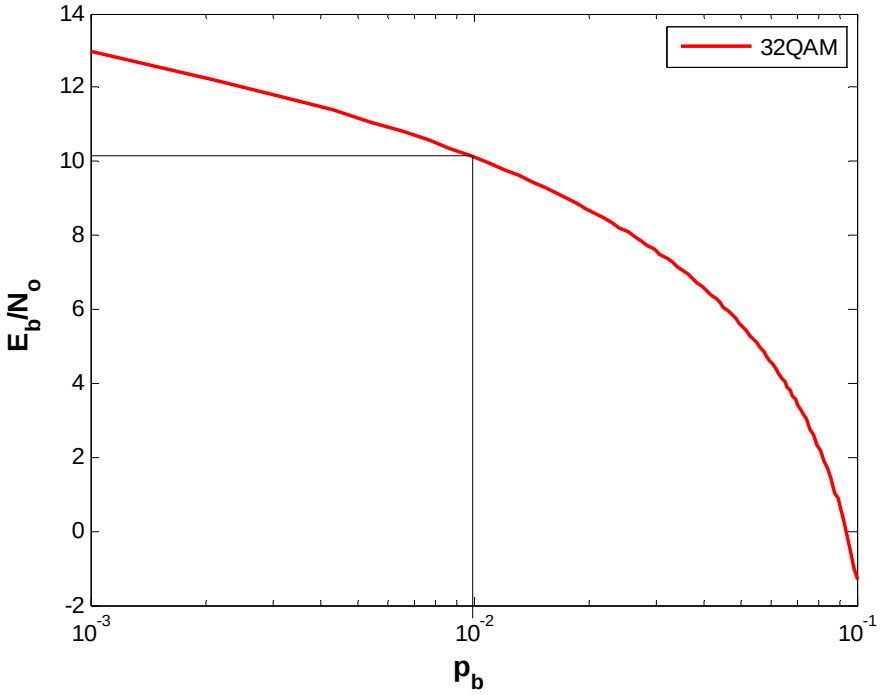

Figure 11. 32-QAM performance for a non-fading channel.

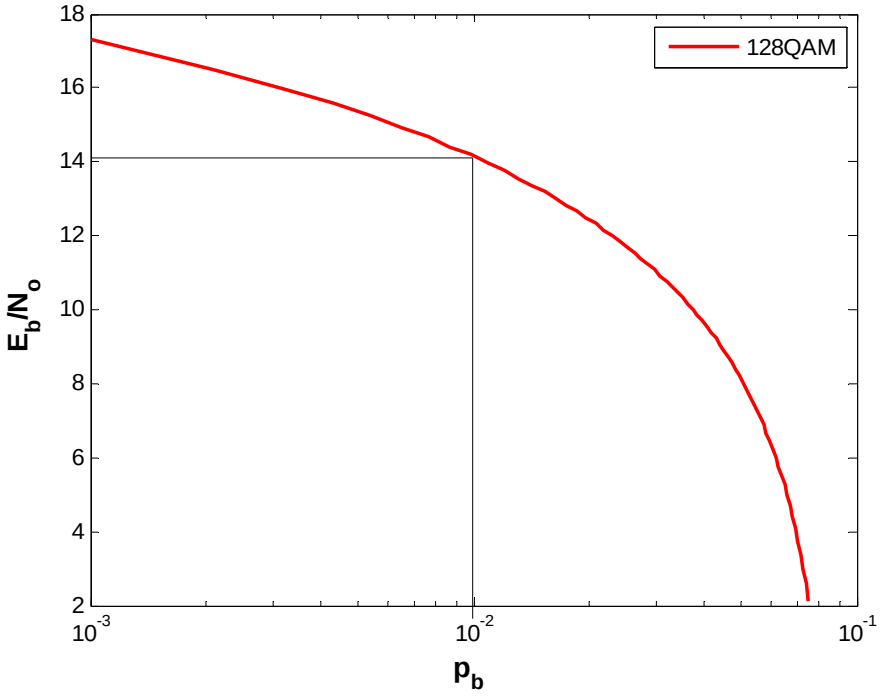

Figure 12. 128-QAM performance for a non-fading channel.

3. GMSK

GMSK is used for the European wireless standard Global System for Mobile (GSM) [6]. As the military becomes joint in nature, it is also expected that increasing coordination with other nations will follow. Thus, it is important to explore standards and implementations other than our own. The wireless communication industry is always exploring ways to incorporate global standards. This is evident, as seen in the transition from dual band cellular phones to the quad-band phones currently available. Even with the advent of these technologies there is much research that continues in an attempt to merge wireless standards.

For GMSK, the modulation constant b varies, as shown in Table 1, with respect to δ. The value for δ varies due to the bandwidth-bit duration product BT_b, but there is only about a one-dB variation in the signal-to-noise ratio required to obtain a specified probability of bit error [2], so for this thesis $\delta = 0.72$ is used, which corresponds approximately to GSM.

Substituting $\gamma_{b\min} = 10^{0.25}$ and the appropriate parameters from Table 1, we get

$$\gamma_b = 10\log\left[-1.4\ln\left(\sqrt{1.44\pi \times 10^{0.25}}\right)p_b\right] \tag{3.12}$$

for GMSK. Equation (3.12) is plotted in Figure 13. A γ_b of 5.7 dB is required to obtain a probability of channel bit error of 10^{-2}.

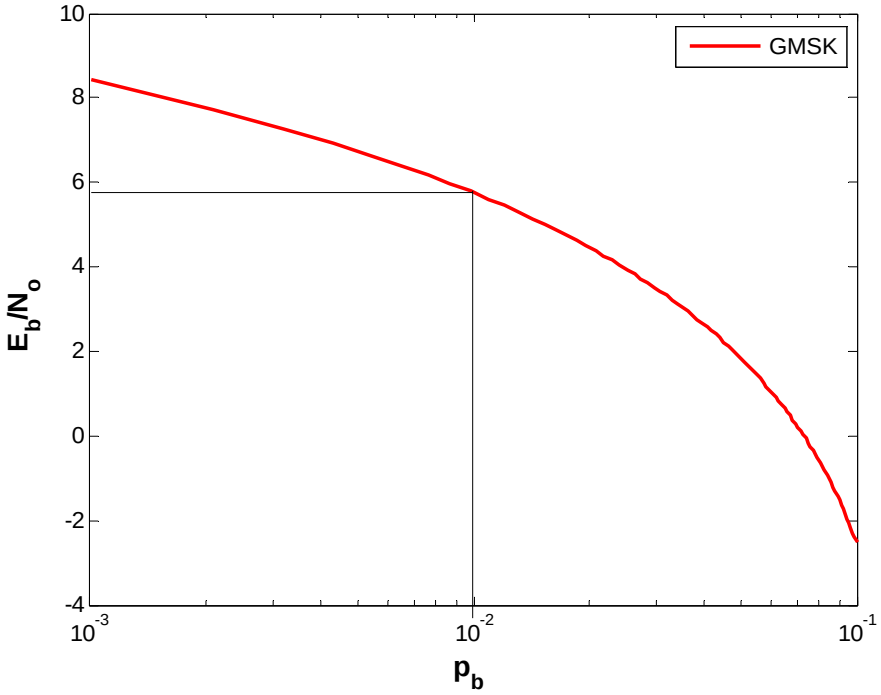

Figure 13. GMSK performance for a non-fading channel.

B. NONCOHERENT MODULATION, *M*-ARY ORTHOGONAL SIGNALING

M-ary orthogonal signaling such as *M*FSK is a modulation used for both commercial and military communications. *M*FSK is used in Milstar, a U.S. Military satellite communications system. In addition, *M*-ary orthogonal signaling is used for the reverse channel of the IS-95 wireless standard [3]. Although 8-FSK, 16-FSK and 32-FSK are shown in this work, it is important to note that noncoherent, *M*-ary orthogonal modulation techniques have identical performance.

Evaluating the performance of *M*FSK is rather trivial when compared to the coherent techniques discussed earlier. By inverting Equation (2.4), repeated here for convenience,

$$p_b \approx \frac{M}{4}\exp\left(-q\gamma_b/2\right), \tag{3.13}$$

where $M = 2^q$, we get

$$\gamma_b = 10\log\left(-\frac{2}{q}\ln\left(\frac{4}{M}\right)p_b\right). \tag{3.14}$$

From Equation (3.14), we get (3.15) for 8-FSK

$$\gamma_b = \left[10\log\left(-0.67\ln\left(0.5\right)p_b\right)\right]. \tag{3.15}$$

Similarly, for 16-FSK

$$\gamma_b = \left[10\log\left(-0.5\ln\left(0.25\right)p_b\right)\right], \tag{3.16}$$

and for 32-FSK,

$$\gamma_b = \left[10\log\left(-0.4\ln\left(0.125\right)p_b\right)\right]. \tag{3.17}$$

Equations (3.15), (3.16) and (3.17) are plotted in Figures 14, 15 and 16, respectively. As can be seen, a γ_b of 5.5 dB, 4.7 dB and 4.3 dB is required for $p_b = 10^{-2}$ for 8-FSK, 16-FSK and 32-FSK, respectively.

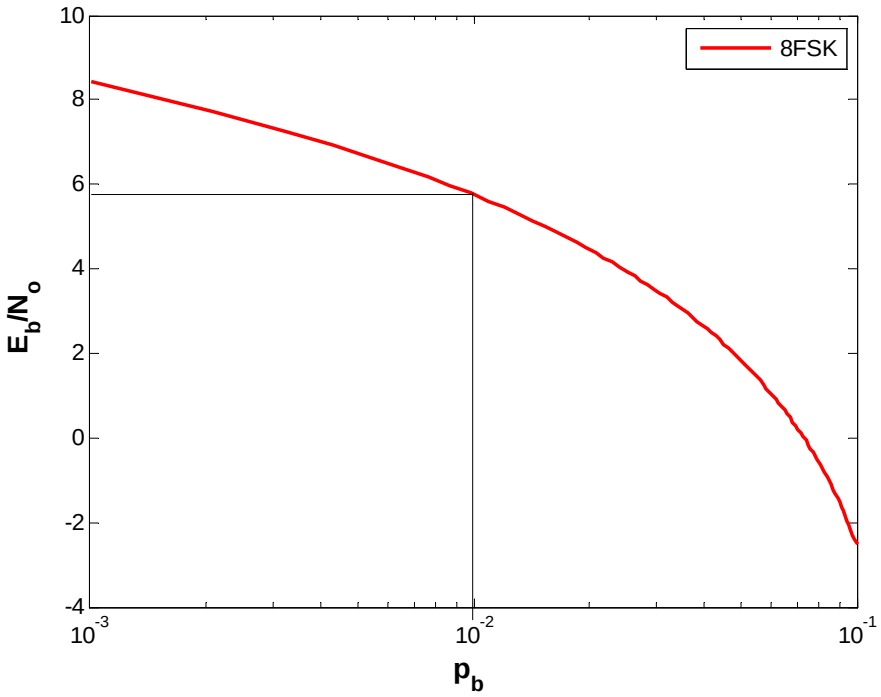

Figure 14. 8-FSK performance for a non-fading channel.

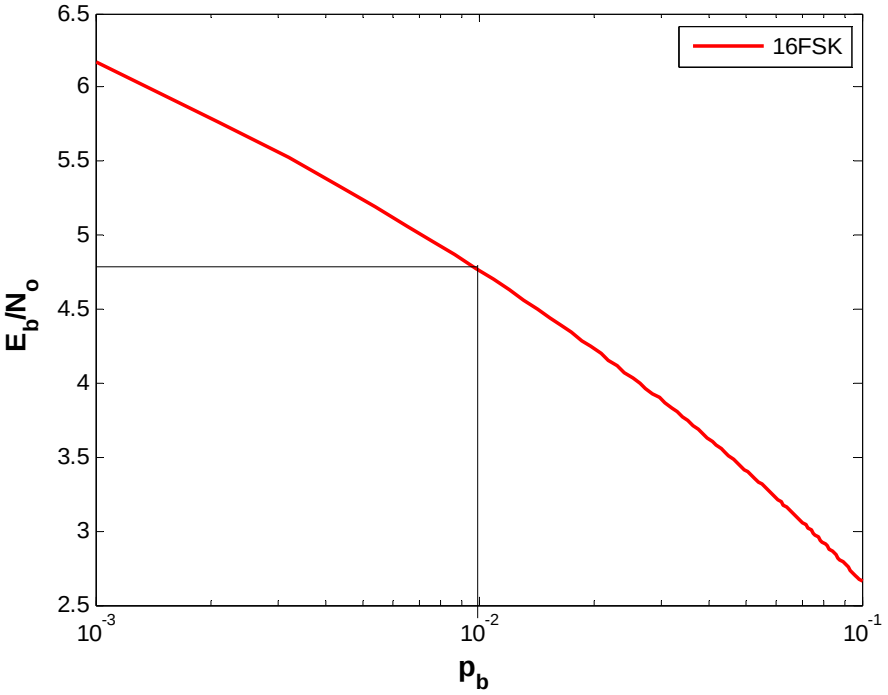

Figure 15. 16-FSK performance for a non-fading channel.

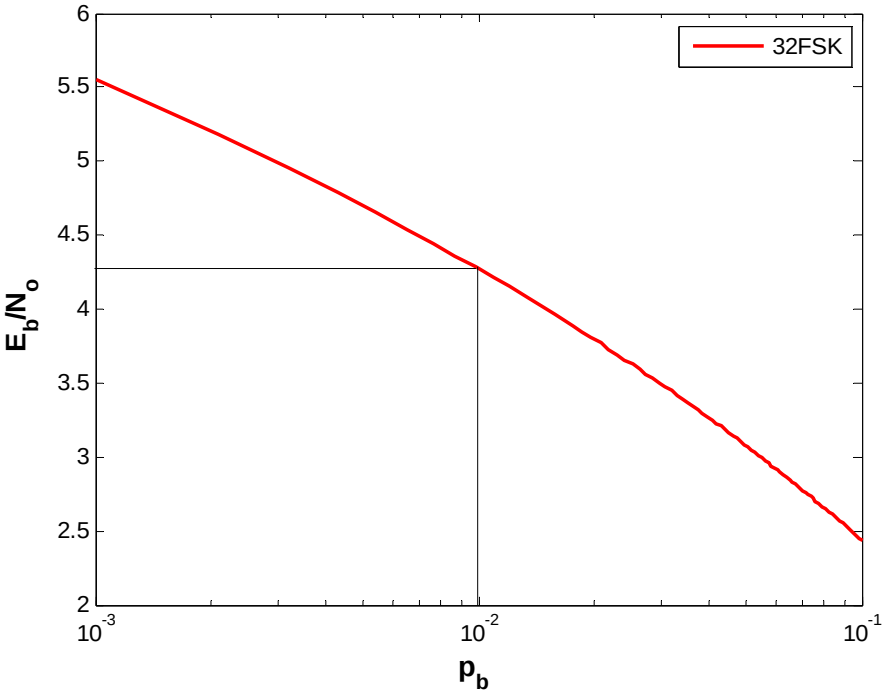

Figure 16. 32-FSK performance in a non-fading channel.

In contrast to the coherent modulation techniques evaluated, noncoherent *M*FSK differs in that, as M increases, the required signal-to-noise ratio decreases [3].

Expressions for the signal-to-noise ratio as functions of the probability of channel bit error were developed in this chapter. The next chapter extends the expressions to encompass the effects of Rayleigh fading channels for the various modulation techniques being considered.

IV. SLOW, FLAT RAYLEIGH FADING CHANNELS

A slow, flat Rayleigh fading channel is a model of a communications channel that is used when there is no line-of-sight between the transmitter and the receiver, and all of the received signal power is due to multipath. In contrast to no fading, this model represents the opposite end of the spectrum. For coherent modulation techniques, the probability of bit error for a slow, flat Rayleigh fading channel is obtained from Equation (2.5) with $\alpha = 0$, which results in [2] Equation Chapter (Next) Section 4

$$p_b = \frac{a}{q}\int_0^\infty Q(\sqrt{b\gamma_s})\frac{\sigma_0^2}{2\sigma^2}\exp\left(\frac{-\gamma_s\sigma_0^2}{2\sigma^2}\right)d\gamma_s \tag{4.1}$$

where

$$\gamma_b = \frac{E_b}{N_0} = \frac{\gamma_s}{q}. \tag{4.2}$$

For Rayleigh fading channels, Equation (4.1) can be evaluated, and for each coherent modulation technique considered in this thesis, the analytical expression obtained by evaluating Equation (4.1) can be algebraically inverted. Logarithmic regression is applied to *M*FSK since algebraic inversion is impractical in this case. The same modulation schemes examined for non-fading channels are evaluated for Rayleigh fading channels.

A. COHERENT MODULATION

1. BPSK/QPSK

For BPSK and QPSK and a Rayleigh fading channel, Equation (4.1) can be evaluated to obtain

$$p_b = \frac{1}{2}\left(1-\sqrt{\frac{\gamma_b}{1+\gamma_b}}\right). \tag{4.3}$$

Equation (4.3) can be algebraically inverted to obtain

$$\gamma_b = 10\log\left(\frac{(1-2p_b)^2}{4p_b-4{p_b}^2}\right) \tag{4.4}$$

where the result is expressed in dB and plotted in Figure 17.

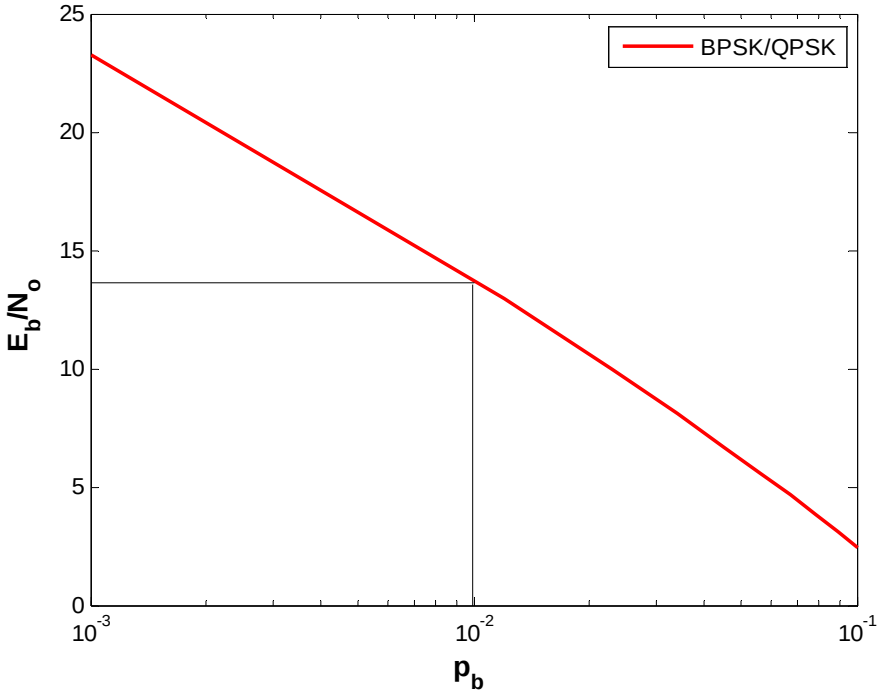

Figure 17. BPSK/QPSK performance for a Rayleigh fading channel.

The performance for BPSK/QPSK for a Rayleigh fading channel exhibits the expected performance degradation when compared to the non-fading channel performance. In order to obtain a probability of channel bit error of $p_b = 10^{-2}$, 14 dB of signal power is required. This is significantly more than the 4.3 dB required for a non-fading environment.

2. *M*PSK

Evaluating Equation (4.1) for *M*PSK and Rayleigh fading, we get [2]

$$p_b = \frac{1}{q}\left(1 - \sqrt{\frac{q\gamma_b \sin^2(\pi/M)}{1 + q\gamma_b \sin^2(\pi/M)}}\right) \tag{4.5}$$

In order to meet demands for current applications, both 8-PSK and 16-PSK were evaluated with satisfactory results. After inverting Equation (4.5) for 8-PSK and 16-PSK, we get

$$\gamma_b = 10\log\left(\frac{1}{8\sin^2(\pi/8)}\right)\left(\frac{(1-8p_b)^2}{16p_b - 64{p_b}^2}\right) \tag{4.6}$$

for 8-PSK and

$$\gamma_b = 10\log\left(\frac{1}{16\sin^2(\pi/16)}\right)\left(\frac{(1-16p_b)^2}{32p_b - 256{p_b}^2}\right) \tag{4.7}$$

for 16-PSK. Equations (4.6) and (4.7) are plotted in Figures 18 and 19, respectively.

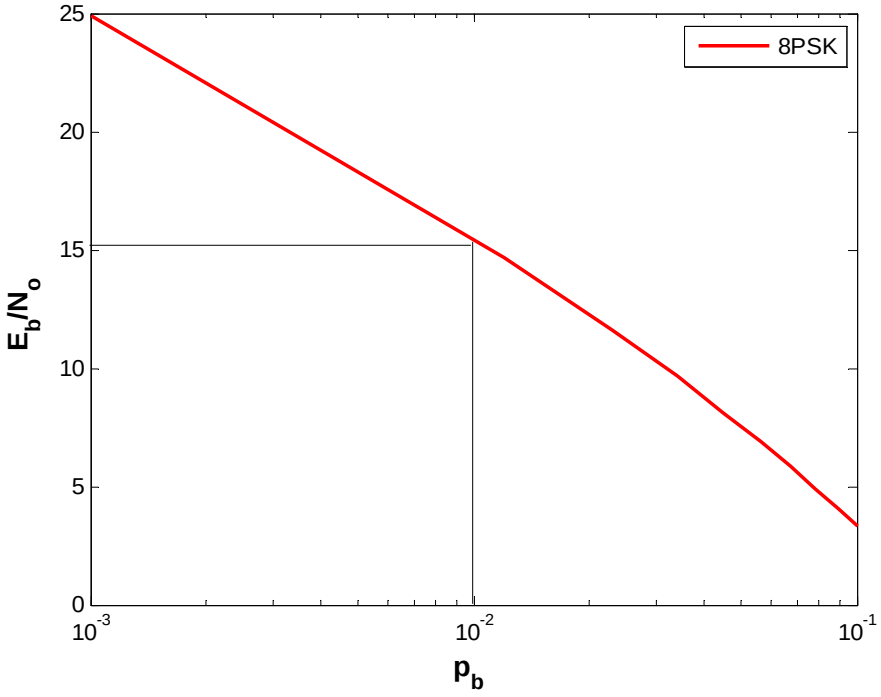

Figure 18. 8-PSK performance for a Rayleigh fading channel.

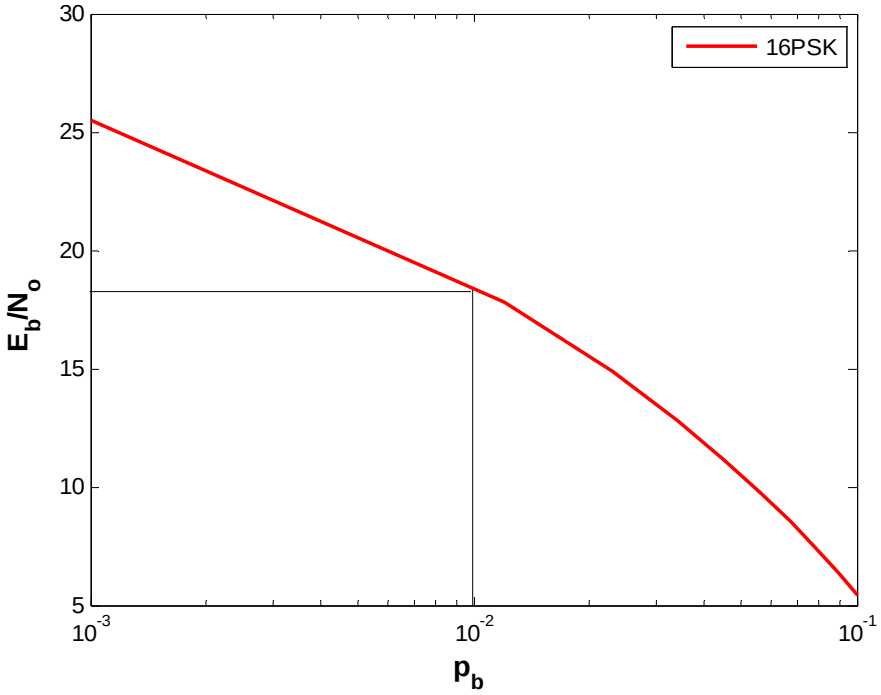

Figure 19. 16-PSK performance for a Rayleigh fading channel.

For 8-PSK and 16-PSK, for a channel p_b of 10^{-2}, E_b/N_o of 15.5 dB and 18.6 dB, respectively, are required. As expected, the E_b/N_o required increases when no line-of-sight exists. This is an increase from the values of 9.7 dB and 15.5 dB, respectively, for 8-PSK and 16-PSK in a non-fading channel.

3. *M*QAM

As described for a non-fading channel model, for *M*QAM it is necessary to examine *M*QAM for two variations of the modulation-type parameters, one when q is even and one when q is odd as seen in Table 1. Although both modulation-type parameters provide good results, the q-even modulation-type parameters produce slightly more accurate results [4]. Analyzing 16-QAM and 64-QAM are important because they are used in the IEEE 802.11g wireless standard [6].

For *M*QAM with even q, Equation (4.1) can be evaluated to obtain

$$p_b = \frac{2}{q}\left(1-2^{\frac{-q}{2}}\right)\left(1-\sqrt{\frac{3q\gamma_b}{2(2^q-1)+3q\gamma_b}}\right). \tag{4.8}$$

After inverting Equation (4.8), we obtain the result for 16-QAM as

$$\gamma_b = 10\log\left(\frac{5}{2}\right)\left(\frac{(1-(8/7)\,p_b)^2}{(16/7)\,p_b-(64/49)\,p_b{}^2}\right) \tag{4.9}$$

which is plotted in Figure 20. As can be seen, $E_b/N_o = 10$ dB is required for $p_b = 10^{-2}$.

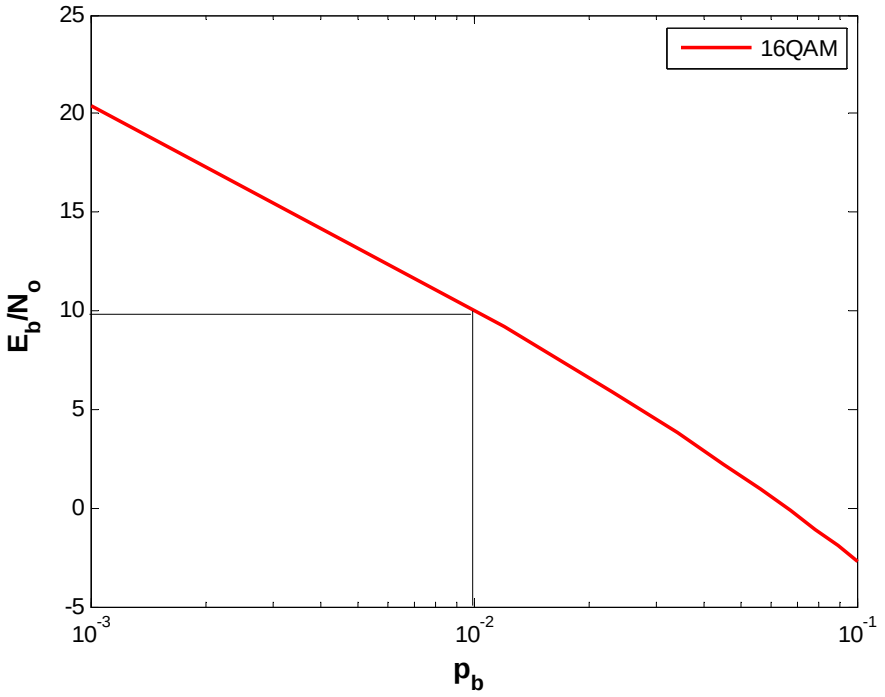

Figure 20. 16-QAM performance for a Rayleigh fading channel.

The same method was applied to 64-QAM. The result is given by

$$\gamma_b = 10\log 7\left(\frac{(1-(24/7)\,p_b)^2}{(48/7)\,p_b-(576/49)\,p_b{}^2}\right) \tag{4.10}$$

which is plotted in Figure 21. As can be seen, $E_b/N_o = 16.4$ dB is required for $p_b = 10^{-2}$.

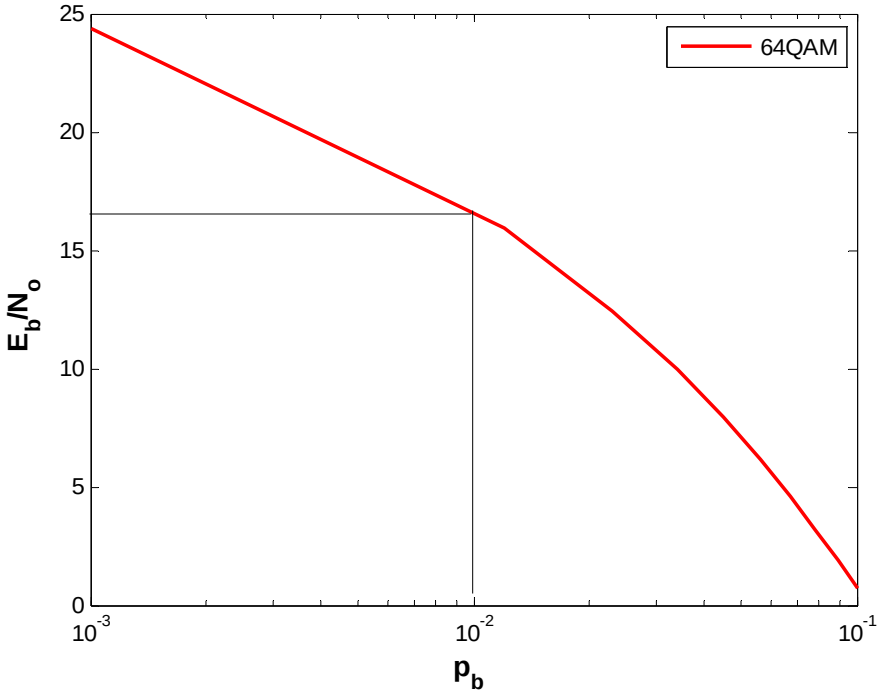

Figure 21. 64-QAM performance for a Rayleigh fading channel.

Despite its limited use in many practical applications, 256-QAM was also evaluated. However, it does provide an insight into the power that is required when this modulation technique is used. Using the same methodology as previously, we invert Equation (4.8) with $M = 256$ to obtain

$$\gamma_b = 10\log\left(\frac{510}{24}\right)\left(\frac{(1-(64/15)\,p_b)^2}{(128/15)\,p_b - (4096/225)\,p_b^{\,2}}\right) \tag{4.11}$$

which is plotted in Figure 22. As can be seen, $E_b/N_o = 20$ dB is required for $p_b = 10^{-2}$.

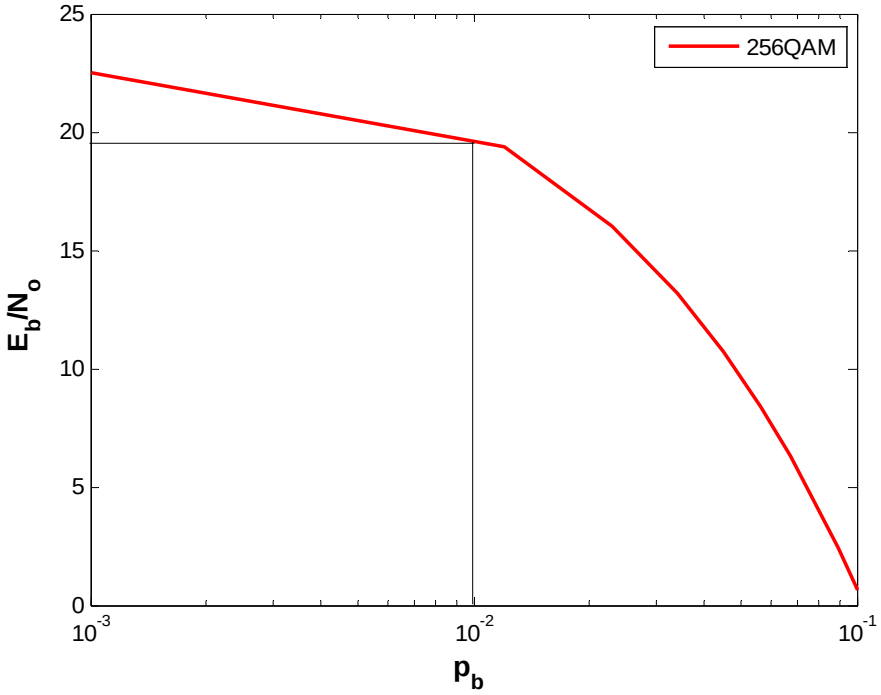

Figure 22. 256-QAM performance for a Rayleigh fading channel.

*M*QAM was also evaluated for odd values of q. For *M*QAM with q as an odd value that is greater than or equal to 3, Equation (4.1) can be evaluated to obtain [2]

$$p_b = \frac{2}{q}\left(1 - \sqrt{\frac{3q\gamma_b}{2(2^q - 1) + 3q\gamma_b}}\right). \tag{4.12}$$

Utilizing the same concept as for even values of q, we obtained inverted equations for 8-QAM, 32-QAM and 128-QAM. Inverting Equation (4.12) for 8-QAM, we get

$$\gamma_b = 10\log\frac{14}{9}\left(\frac{(1-(3/2)\,p_b)^2}{3p_b - (9/4)\,p_b^{\,2}}\right) \tag{4.13}$$

which is plotted in Figure 23. As can be seen, $E_b/N_o = 17$ dB is required for $p_b = 10^{-2}$.

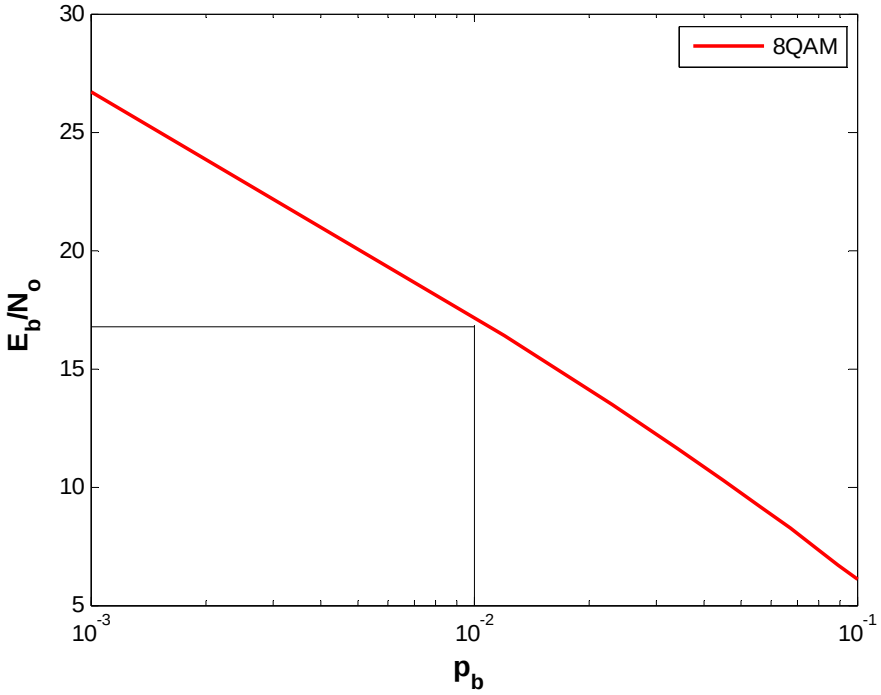

Figure 23. 8-QAM performance for a Rayleigh fading channel.

Similarly, for 32-QAM we get

$$\gamma_b = 10\log\frac{62}{15}\left(\frac{(1-(5/2)\,p_b)^2}{5\,p_b-(25/4)\,p_b{}^2}\right) \tag{4.14}$$

which is plotted in Figure 24. As can be seen, $E_b/N_o = 19$ dB is required for $p_b = 10^{-2}$.

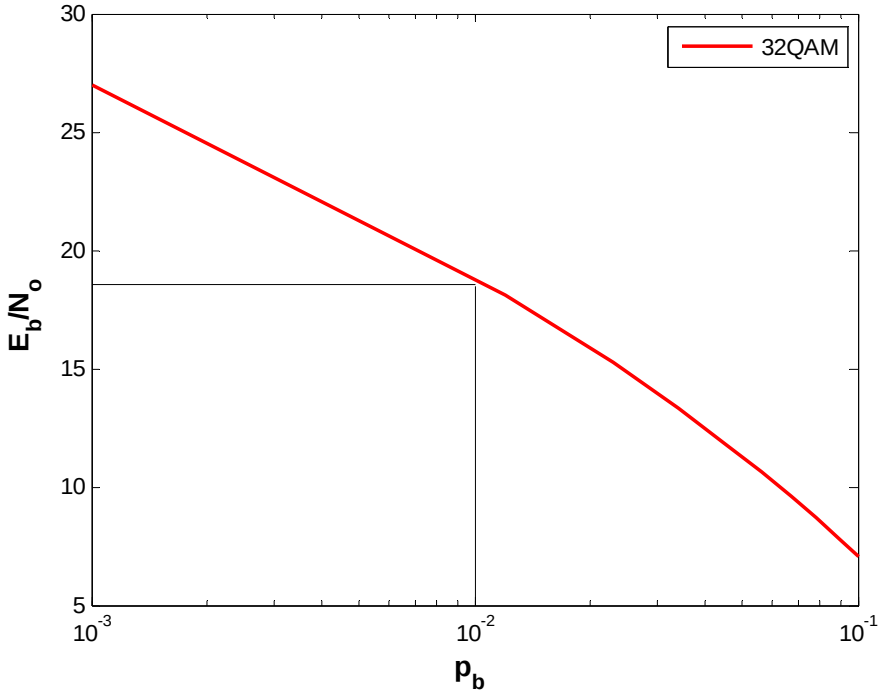

Figure 24. 32-QAM performance for a Rayleigh fading channel.

Again as before, for 128-QAM, we get

$$\gamma_b = 10\log\frac{254}{21}\left(\frac{(1-(7/2)\,p_b)^2}{7\,p_b-(49/4)\,{p_b}^2}\right), \tag{4.15}$$

which is plotted in Figure 25. As can be seen, $E_b/N_o = 21$ dB is required for $p_b = 10^{-2}$.

As q increases, as expected, the signal-to-noise ratio required for a given channel bit error performance increases [3].

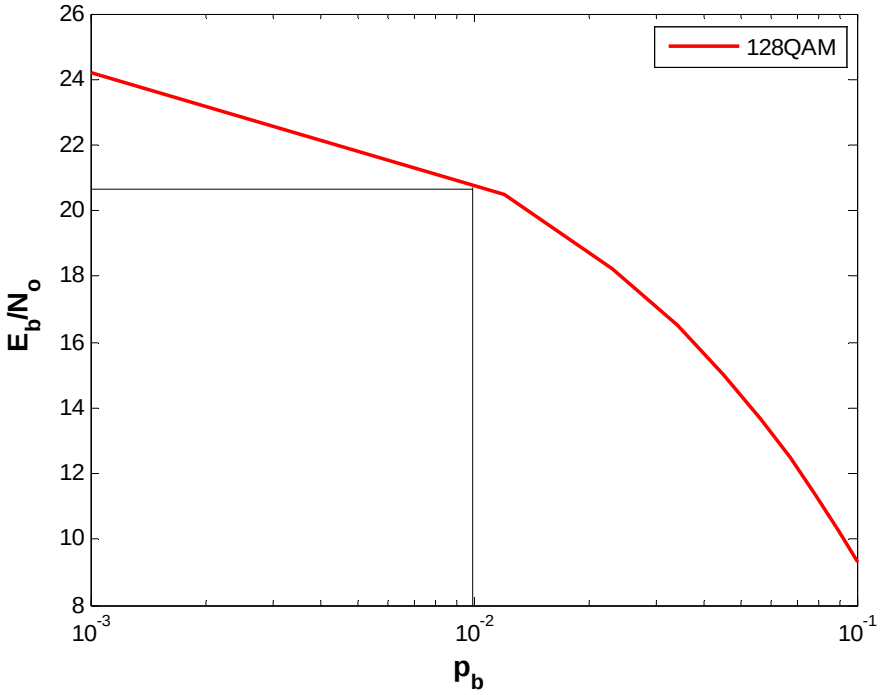

Figure 25. 128-QAM performance for a Rayleigh fading channel.

4. GMSK

The same algebraic inversion technique was used to invert the GMSK expression for a Rayleigh fading channel. Just as in the non-fading case, $b = 2\delta$, where $\delta = 0.72$, was used. Evaluating Equation (4.1) for GMSK, we get [2]

$$p_b = \frac{1}{2}\left(1 - \sqrt{\frac{\delta\gamma_b}{1+\delta\gamma_b}}\right). \tag{4.16}$$

Equation (4.16) can be inverted to obtain

$$\gamma_b = 10\log\frac{1}{\delta}\left(\frac{(1-2p_b)^2}{4p_b - 4p_b^{\,2}}\right) \tag{4.17}$$

which is plotted in Figure 26. As can be seen, $E_b/N_o = 15.4\,\text{dB}$ is required for $p_b = 10^{-2}$.

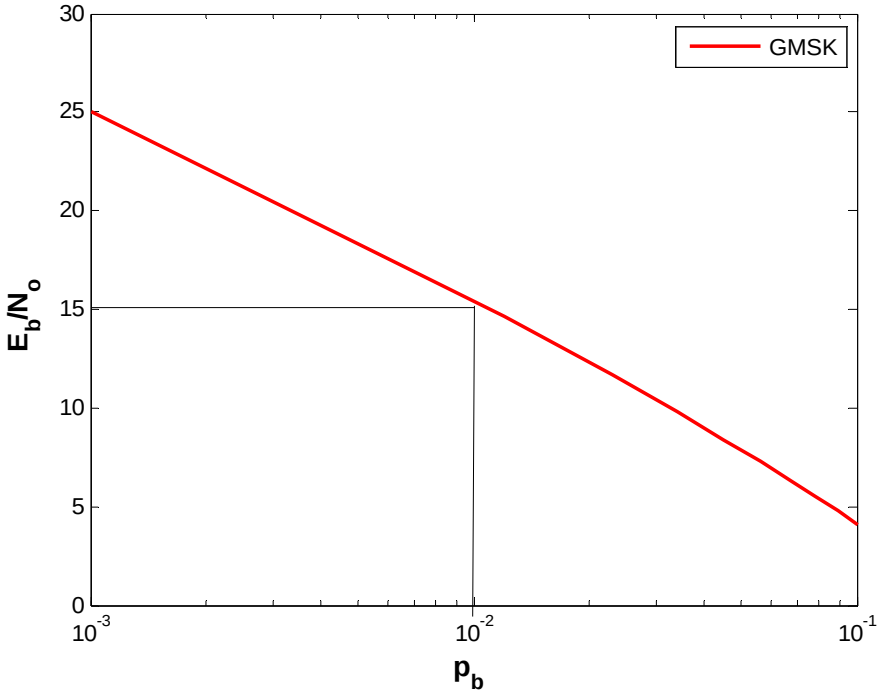

Figure 26. GMSK performance for a Rayleigh fading channel.

B. NONCOHERENT MODULATION, *M*-ARY ORTHOGONAL SIGNALING

*M*FSK, and *M*-ary orthogonal signaling in general, are the noncoherent modulation techniques evaluated in this thesis. We will evaluate 8-FSK, 16-FSK and 32-FSK because they are the most commonly used in practice [4]. Since the expression for *M*FSK and Rayleigh fading cannot be inverted analytically, a logarithmic regression technique is used to get equations for γ_b in terms of p_b. This logarithmic regression technique was used in cases where algebraic inversion is impractical. The probability of channel bit error for *M*FSK transmitted over a Rayleigh fading channel is given by [2]

$$p_b = \frac{M}{2(M-1)} \sum_{n=1}^{M-1} \frac{(-1)^{n+1}}{(1+n+nq\gamma_b)} \binom{M-1}{n}. \tag{4.18}$$

The exact expression is used since the union bound is inaccurate for Rayleigh fading channels [4].

Using the logarithmic regression technique on Equation (4.18) when $M = 8$, $M = 16$ and $M = 32$, we get

$$\gamma_b = \left[-3.9 \ln(p_b) - 9.1\sqrt{p_b} - 0.008 \right] \tag{4.19}$$

for 8-FSK,

$$\gamma_b = \left[-4.1 \ln(p_b) - 7.1\sqrt{p_b} - 1.5 \right], \tag{4.20}$$

for 16-FSK and

$$\gamma_b = \left[-4 \ln(p_b) - 6.7\sqrt{p_b} - 1.7 \right] \tag{4.21}$$

for 32-FSK.

Equations (4.19), (4.20) and (4.21) are plotted in Figures 27, 28 and 29, respectively. As can be seen, $E_b/N_o = 16.7$ dB, $E_b/N_o = 16.3$ dB and $E_b/N_o = 15.8$ dB are required to achieve $p_b = 10^{-2}$ for $M = 8$, 16 and 32, respectively. Similarly, if necessary, γ_b can be obtained for $M \geq 64$. As expected, as M increases, the required γ_b decreases.

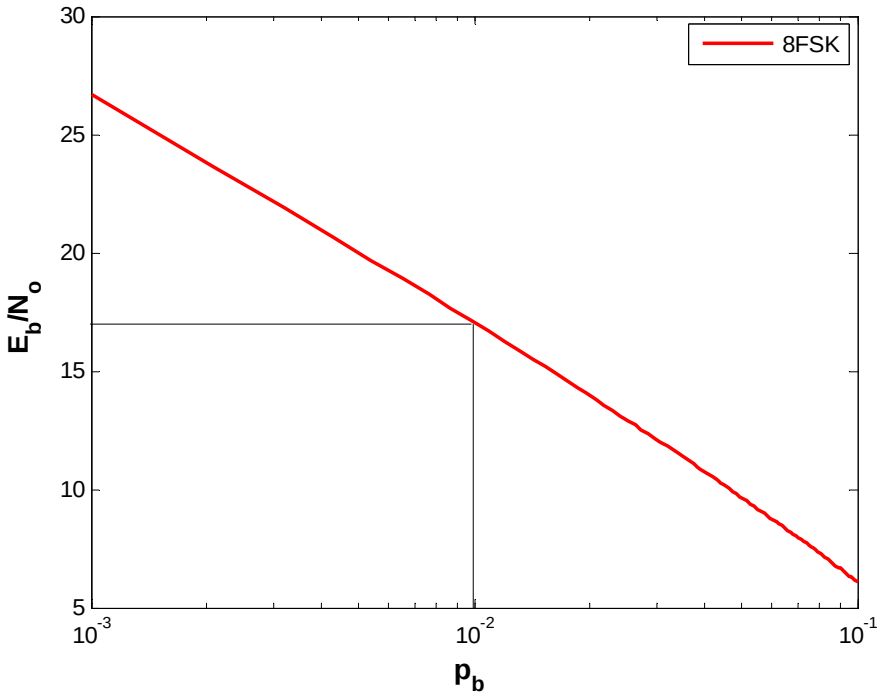

Figure 27. 8-FSK performance for a Rayleigh fading channel.

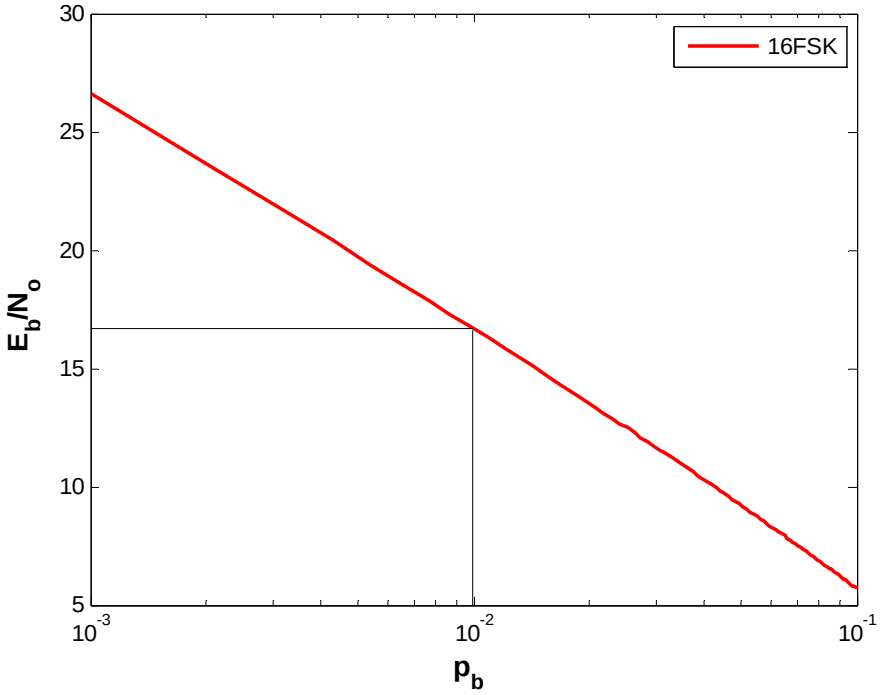

Figure 28. 16-FSK performance for a Rayleigh fading channel.

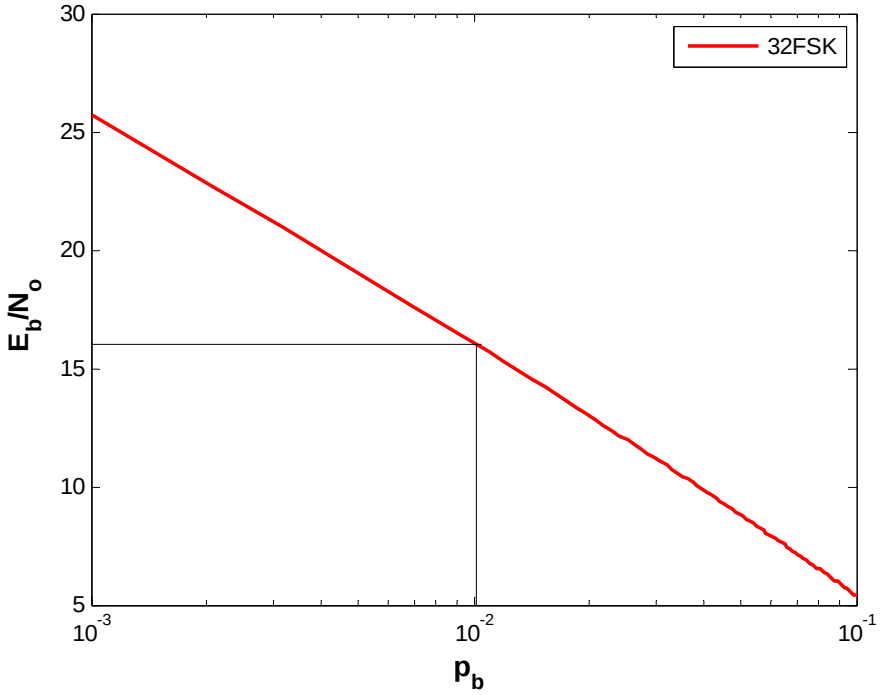

Figure 29. 32-FSK performance for a Rayleigh fading channel.

Expressions for the signal-to-noise ratio as functions of the probability of channel bit error for Rayleigh fading channels were developed in this chapter. The next chapter repeats the process for Ricean fading channels.

V. SLOW, FLAT RICEAN FADING CHANNELS

The slow, flat Ricean model is used where there is a line-of-sight between transmitter and receiver but a substantial portion of the received signal power is also due to multipath. The most noticeable difference in the equations for a Ricean channel is the direct-to-diffuse signal power ratio ζ. As ζ increases, the model tends to approach a non-fading model. In contrast, as ζ approaches 0, the model approaches that of a Rayleigh fading model. Equation Chapter (Next) Section 5

The direct-to diffuse signal power ratio is defined by [2]

$$\zeta = \frac{\alpha^2}{2\sigma^2}, \tag{5.1}$$

where α^2 represents the received line-of-sight signal power, and $2\sigma^2$ is the non-line-of-sight signal power.

For coherent demodulation techniques, the equations for Ricean fading channels are derived from [2]

$$p_b = \frac{a}{q}\int_0^\infty Q(\sqrt{b\gamma_s})\frac{\sigma_0^2}{2\sigma^2}\exp\left[-\frac{(\gamma_s\sigma_0^2+\alpha^2)}{2\sigma^2}\right] I_0\left(\frac{\alpha\sqrt{\gamma_s\sigma_0^2}}{\sigma^2}\right) d\gamma_s, \tag{5.2}$$

where $\gamma_s = q\gamma_b$.

Implementing Equation (5.2) for BPSK and for varying values of the parameter ζ, we obtain the results shown in Figure 30.

In order to invert the equations for Ricean fading channels, the same logarithmic regression technique used for *M*FSK and Rayleigh fading is used.

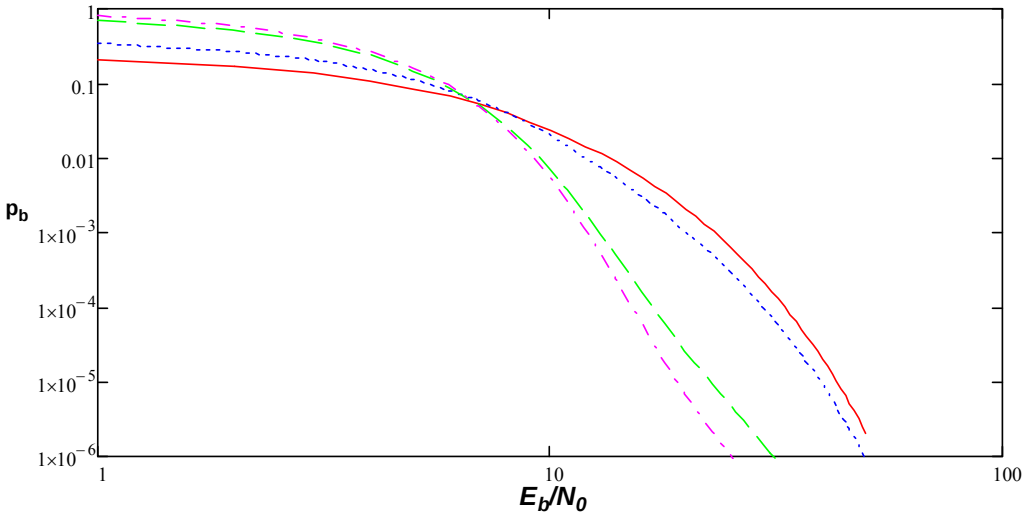

Figure 30. Performance of BPSK transmitted over a Ricean fading channel for $\zeta = 2, 4, 10, 12$. Increasing ζ denoted by reduction in required E_b/N_o for $p_b < 0.01$. Lines converge at approximately $p_b = 0.05$.

For values of ζ greater than 12, the numerical evaluation of Equation (5.2) is impractical. Generally, if the line-of-sight signal strength is more than 12 times that of the non-line-of-sight signal strength, the LOS component dominates the channel, and the effect of fading is not as important. The modulation techniques being considered were evaluated for Ricean fading channels with $\zeta = 2$ and 10 in order to give an idea of the effect of ζ.

Substituting

$$\gamma_s = \frac{\alpha^2}{\sigma_0^{\,2}}\left(\frac{1+\zeta}{\zeta}\right) \tag{5.3}$$

where $\sigma_0^{\,2} = N_0/T_s$, into Equation (5.2), we can evaluate performance in terms of the direct-to-diffuse ratio parameter [2].

For Ricean fading channels [2],

$$p_b \approx \frac{a}{2q\sqrt{\pi c}}\left(\frac{2(1+\zeta)}{2(1+\zeta)+bq\gamma_b}\right)\exp\left[\frac{-b\zeta q\gamma_b}{2(1+q\gamma_b)}\right] \tag{5.4}$$

is a good approximation where $c = 1.0 + 0.1\zeta$.

A. COHERENT MODULATION

1. BPSK/QPSK

For BPSK and QPSK, for a Ricean fading channel, from Equation (5.4) and Table 1,

$$p_b \approx \frac{1}{2\sqrt{\pi c}}\left[\frac{\zeta+1}{\gamma_b+\zeta+1}\right]\exp\left(\frac{-\zeta\gamma_b}{\gamma_b+\zeta+1}\right). \tag{5.5}$$

Equation (5.5) and logarithmic regression is used to obtain

$$\gamma_b = \left[-4\ln(p_b) - 2\sqrt{p_b} - 7\right] \tag{5.6}$$

and

$$\gamma_b = \left[-1.5\ln(p_b) - 8\sqrt{p_b} - 0.006\right] \tag{5.7}$$

for $\zeta = 2$ and $\zeta = 10$, respectively.

Equations (5.6) and (5.7) are plotted in Figures 31 and 32, respectively. As can be seen, $E_b/N_o = 11\,\text{dB}$ and $E_b/N_o = 5.8\,\text{dB}$ are required to achieve $p_b = 10^{-2}$ when $\zeta = 2$ and 10, respectively. As expected, increasing ζ results in a decrease in required signal-to-noise ratio.

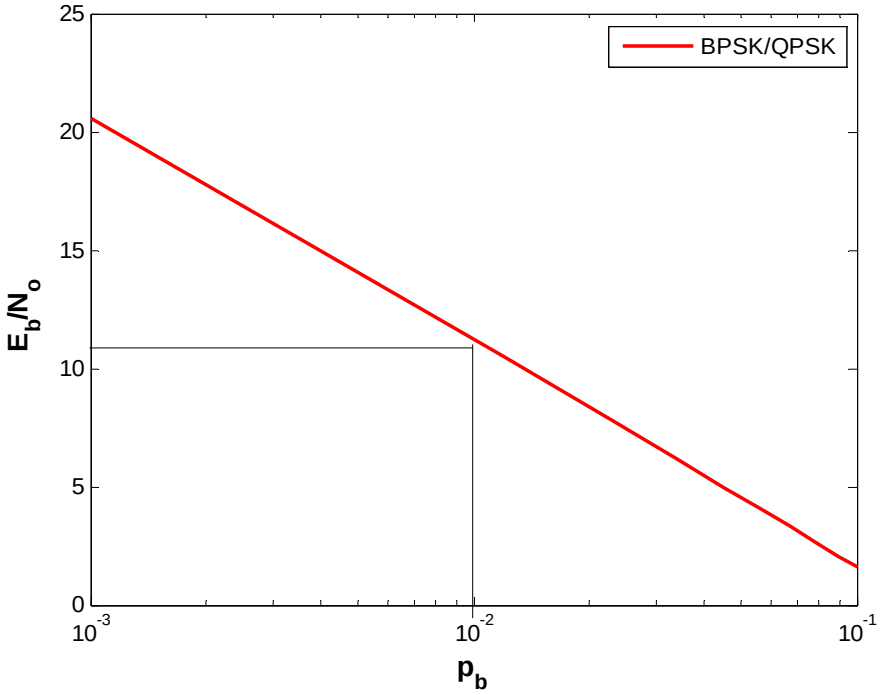

Figure 31. BPSK/QPSK performance for a Ricean fading channel for $\zeta = 2$.

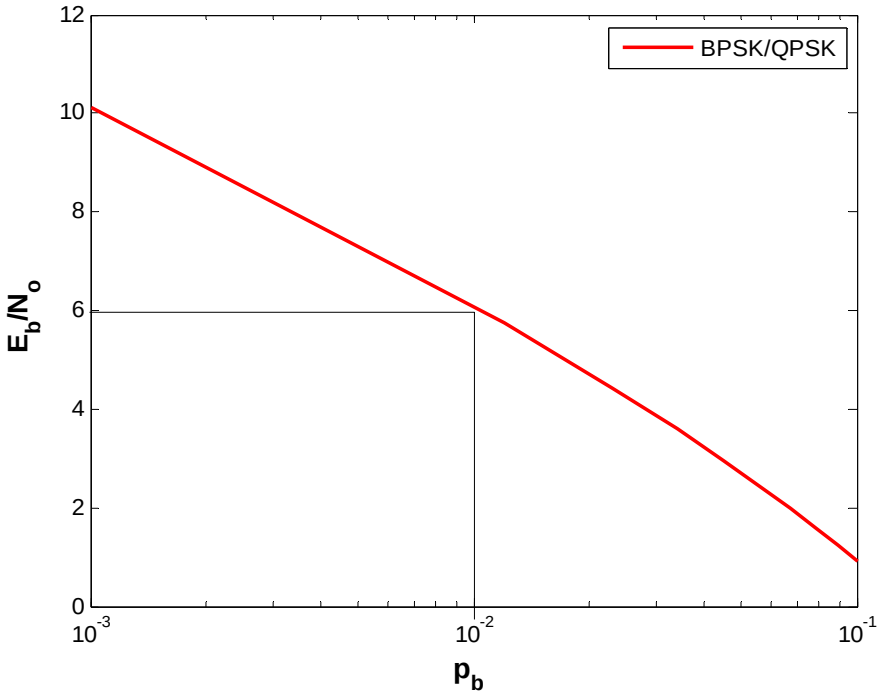

Figure 32. BPSK/QPSK performance for Ricean fading channel for $\zeta = 10$.

2. *M*PSK

For *M*PSK, for a Ricean fading channel from Equation (5.4) and Table 1,

$$p_b \approx \frac{(1+\zeta)}{q\sqrt{\pi c}(1+\zeta+q\sin^2\left(\frac{\pi}{M}\right)\gamma_b} \exp\left[\frac{-q\sin^2\left(\frac{\pi}{M}\right)\zeta\gamma_b}{1+\zeta+q\sin^2\left(\frac{\pi}{M}\right)\gamma_b}\right]. \tag{5.8}$$

Equation (5.8) and logarithmic regression are used to obtain

$$\gamma_b = \left[-2.4\ln(p_b) - 30\sqrt{p_b} + 5.5\right] \tag{5.9}$$

for 8-PSK and $\zeta = 2$ and

$$\gamma_b = \left[-1.3\ln(p_b) - 20\sqrt{p_b} + 4.7\right] \tag{5.10}$$

for 8-PSK and $\zeta = 10$, respectively.

Equations (5.9) and (5.10) are plotted for $\zeta = 2$ and $\zeta = 10$ in Figures 33 and 34, respectively. As can be seen, $E_b/N_o = 13.3\,\text{dB}$ and $E_b/N_o = 8.8\,\text{dB}$ are required to achieve $p_b = 10^{-2}$ for $\zeta = 2$ and 10, respectively.

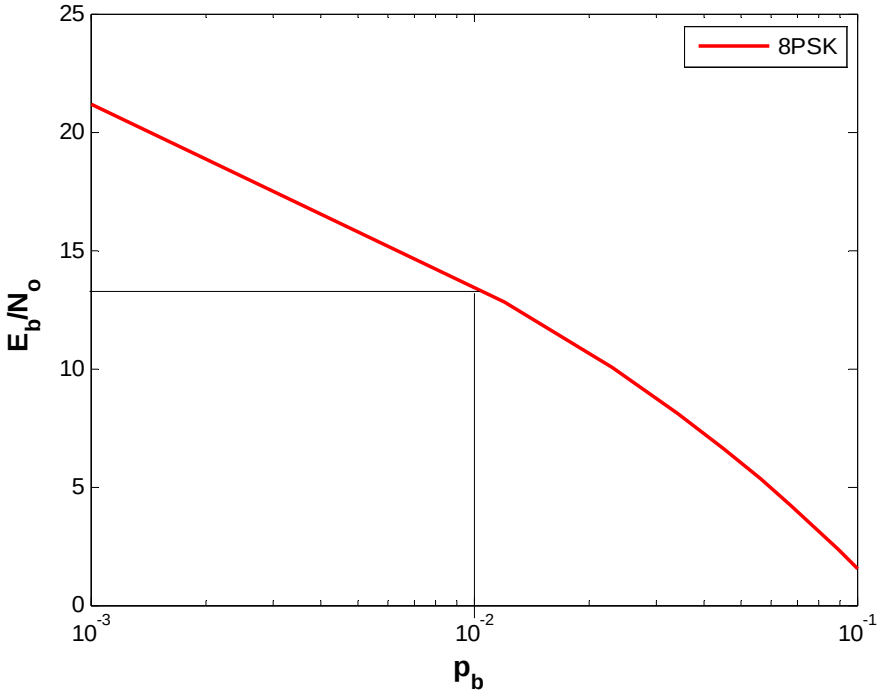

Figure 33. 8-PSK performance for a Ricean fading channel for $\zeta = 2$.

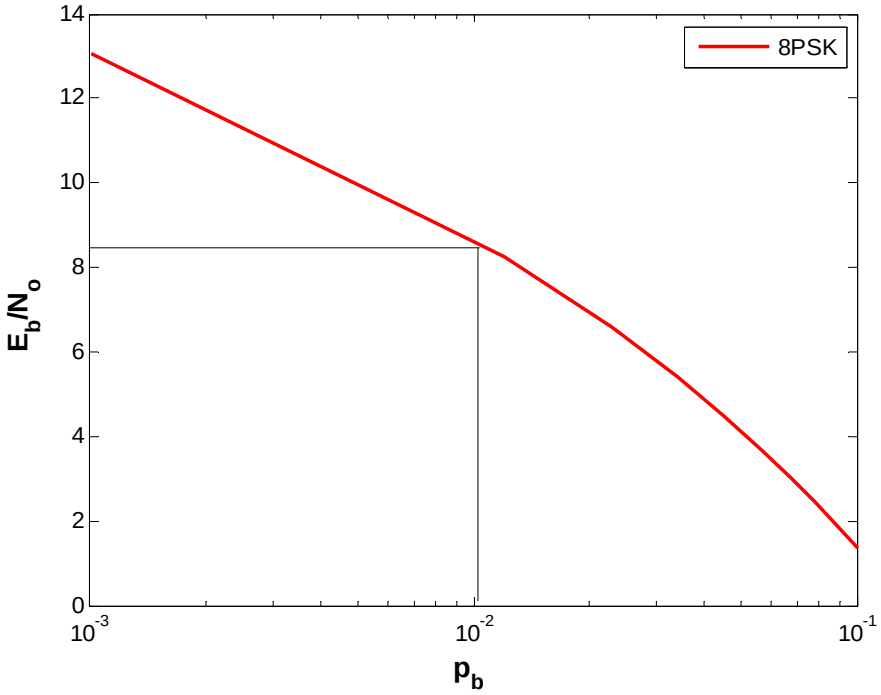

Figure 34. 8-PSK performance for a Ricean fading channel for $\zeta = 10$.

Similarly, the same method was used for 16-PSK. For 16-PSK and a Ricean fading channel,

$$\gamma_b = \left[-2.5 \ln(p_b) - 33\sqrt{p_b} + 8.4 \right] \tag{5.11}$$

when $\zeta = 2$ and

$$\gamma_b = \left[-1.1 \ln(p_b) - 36\sqrt{p_b} + 11 \right] \tag{5.12}$$

when $\zeta = 10$.

Equations (5.11) and (5.12) are plotted in Figures 35 and 36, respectively. As can be seen, $E_b/N_o = 16.8$ dB and $E_b/N_o = 12$ dB are required to achieve $p_b = 10^{-2}$ when $\zeta = 2$ and 10, respectively.

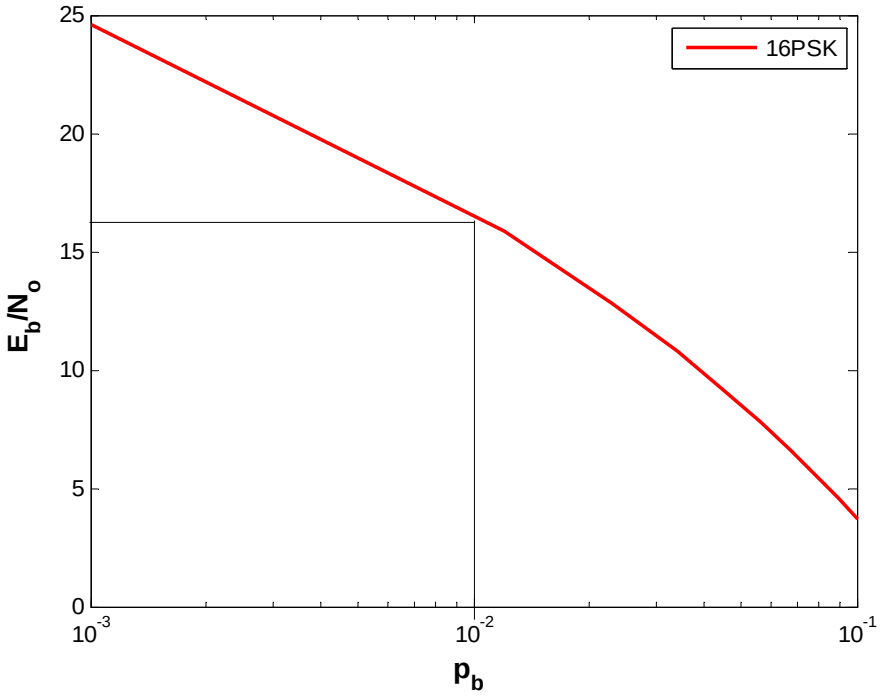

Figure 35. 16-PSK performance in Ricean fading channel for $\zeta = 2$.

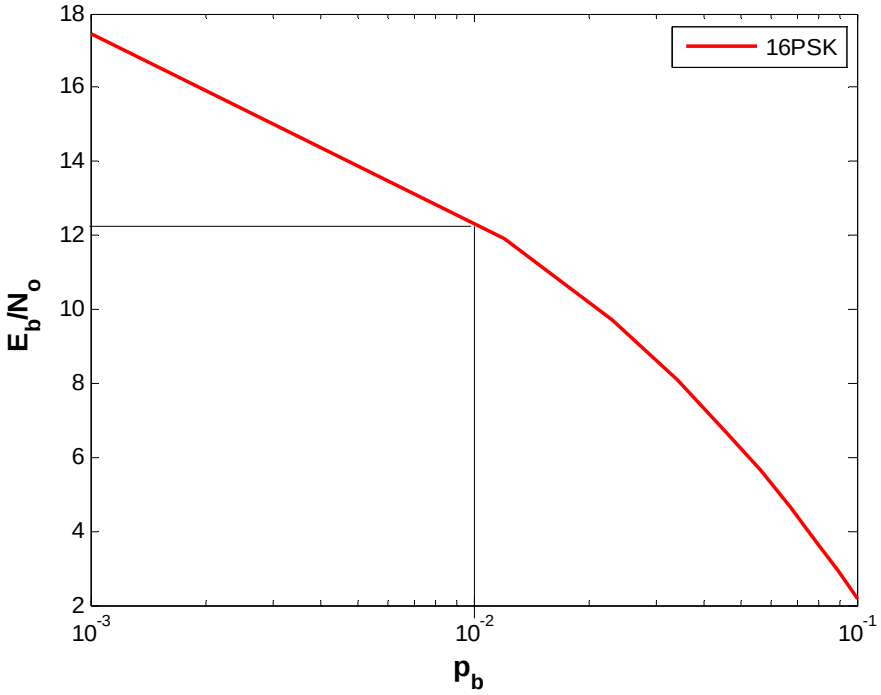

Figure 36. 16-PSK performance for a Ricean fading channel for $\zeta = 10$.

The introduction of the parameter ζ has a big impact on the required signal-to-noise ratio. Based on the value of *M*, there is a wide range of probability of channel bit error that can be introduced into any system as a result of fluctuations in ζ.

3. *M*QAM

*M*QAM for a Ricean fading channel, as previously, is broken down into even and odd values of q. For *M*QAM for a Ricean fading channel and even values of q,

$$p_b \approx \frac{4\left(1-\left(\frac{1}{2^{\frac{q}{2}}}\right)\right)(2^q-1)(\zeta+1)}{q\sqrt{\pi c}\left[3q\gamma_b+2(2^q-1)(\zeta+1)\right]}\exp\left[\frac{-3q\zeta\gamma_b}{3q\gamma_b+2(2^q-1)(\zeta+1)}\right], \qquad (5.13)$$

whereas for odd values of q,

$$p_b \approx \frac{4(2^q-1)(\zeta+1)}{q\sqrt{\pi c}\left[3q\gamma_b+2(2^q-1)(\zeta+1)\right]}\exp\left[\frac{-3q\zeta\gamma_b}{3q\gamma_b+2(2^q-1)(\zeta+1)}\right]. \tag{5.14}$$

Equations (5.13) and (5.14) were evaluated for $\zeta=2$ and $\zeta=10$ for 16-QAM. Inverting Equation (5.13) for even values of q results in

$$\gamma_b=\left[-2.3\ln(p_b)-24\sqrt{p_b}+5.7\right] \tag{5.15}$$

for 16-QAM and $\zeta=2$ and

$$\gamma_b=\left[-1.3\ln(p_b)-11\sqrt{p_b}+1.1\right] \tag{5.16}$$

for 16-QAM and $\zeta=10$.

Equations (5.15) and (5.16) are plotted in Figures 37 and 38, respectively. As can be seen, $E_b/N_o=13$ dB and $E_b/N_o=6$ dB are required to achieve $p_b=10^{-2}$ when $\zeta=2$ and 10, respectively.

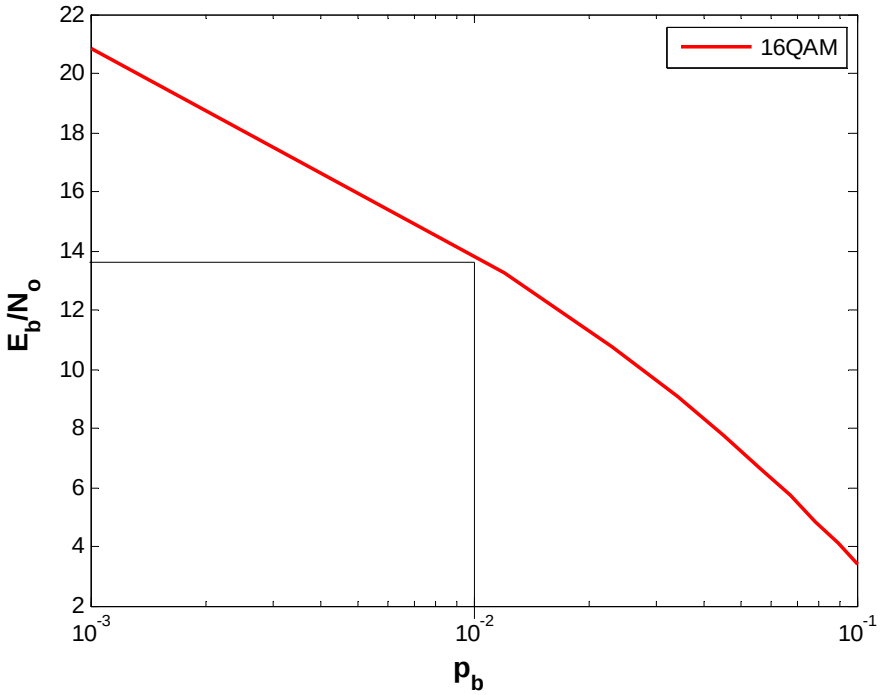

Figure 37. 16-QAM performance for a Ricean fading channel for $\zeta=2$.

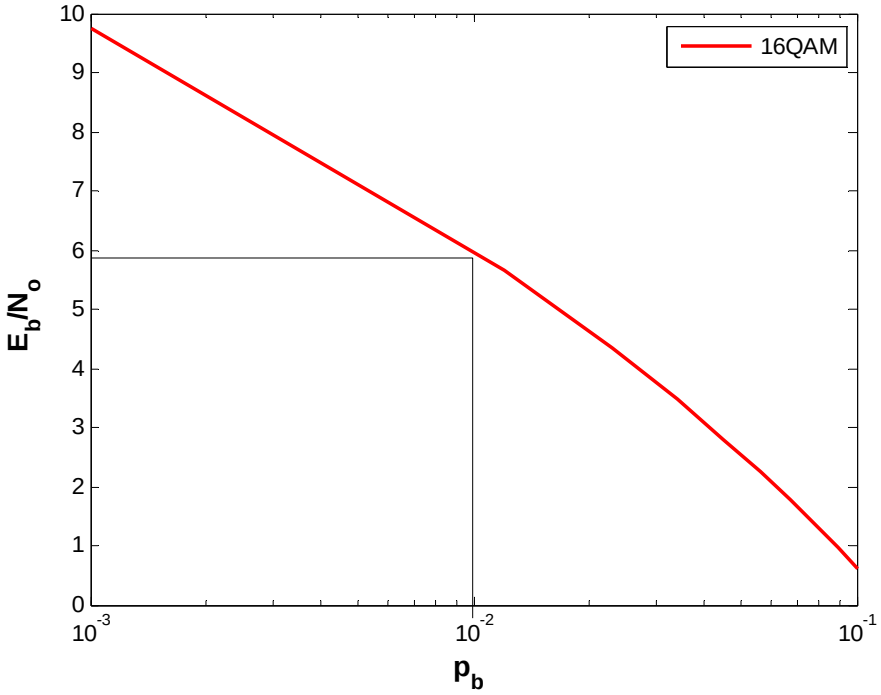

Figure 38. 16-QAM performance for a Ricean fading channel for $\zeta = 10$.

For 64-QAM and $\zeta = 2$, for a Ricean fading channel, we get

$$\gamma_b = \left[0.8 \ln(p_b) - 66\sqrt{p_b} + 27.5 \right], \tag{5.17}$$

and

$$\gamma_b = \left[0.32 \ln(p_b) - 51\sqrt{p_b} + 20 \right] \tag{5.18}$$

for 64-QAM and $\zeta = 10$.

Equations (5.17) and (5.18) are plotted in Figures 39 and 40, respectively. As can be seen, $E_b/N_o = 17$ dB and $E_b/N_o = 13.5$ dB are required to achieve $p_b = 10^{-2}$ when $\zeta = 2$ and 10, respectively.

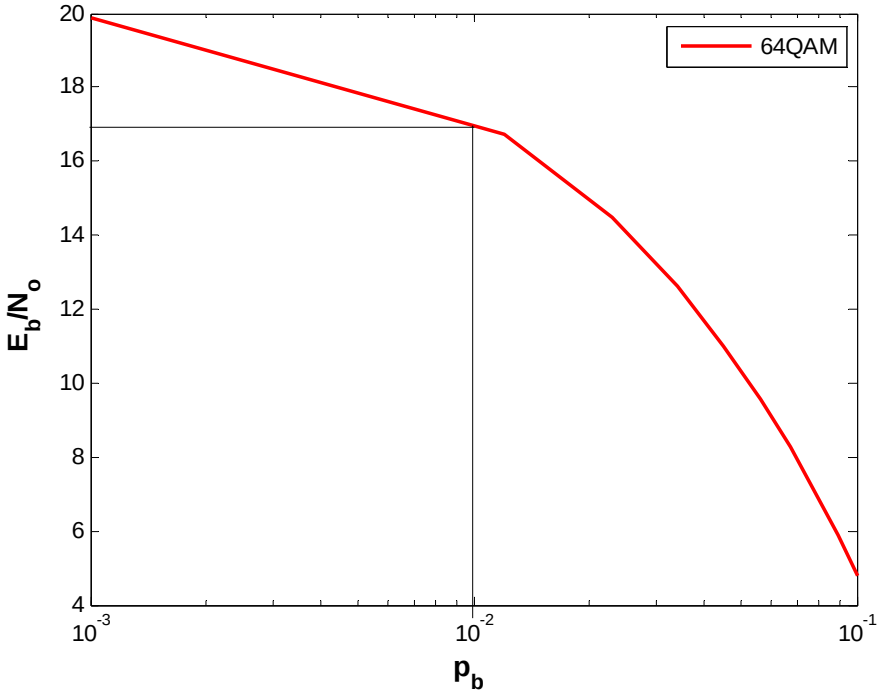

Figure 39. 64-QAM performance for a Ricean fading channel for $\zeta = 2$.

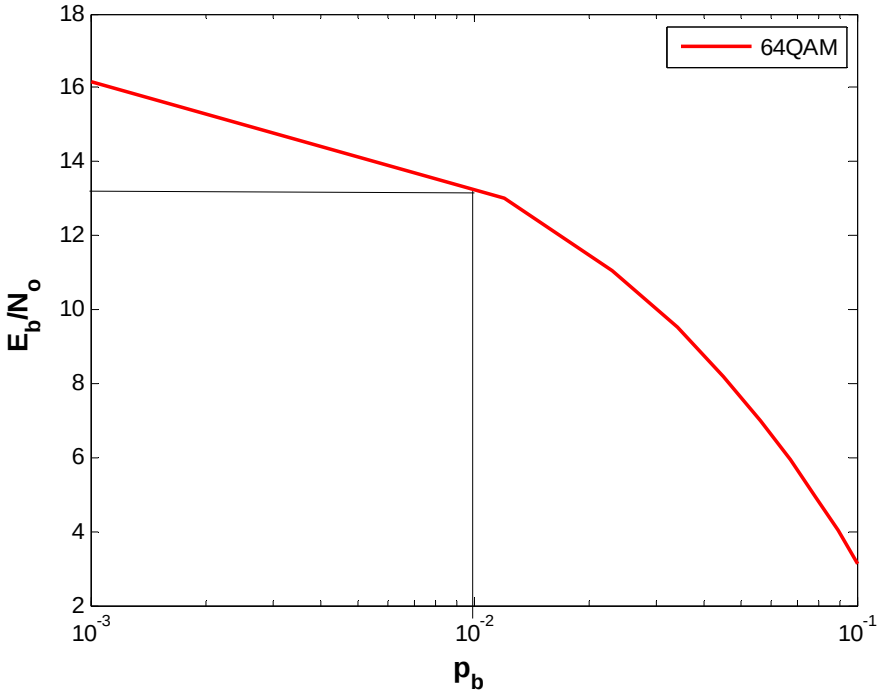

Figure 40. 64-QAM performance for a Ricean fading channel for $\zeta = 10$.

For 256-QAM and $\zeta = 2$, for a Ricean fading channel, we get

$$\gamma_b = \left[0.37 \ln(p_b) - 78\sqrt{p_b} + 32 \right] \tag{5.19}$$

and

$$\gamma_b = \left[-0.3 \ln(p_b) - 62\sqrt{p_b} + 23 \right] \tag{5.20}$$

for 256-QAM and $\zeta = 10$.

Equations (5.19) and (5.20) are plotted in Figures 41 and 42, respectively. As can be seen, $E_b/N_o = 22$ dB and $E_b/N_o = 18$ dB are required to achieve $p_b = 10^{-2}$ when $\zeta = 2$ and 10, respectively.

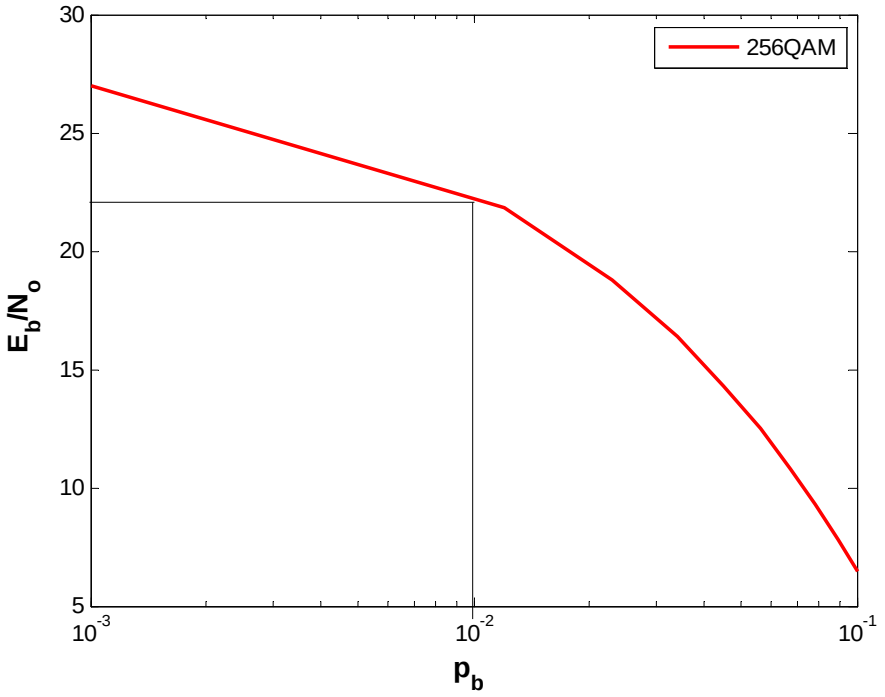

Figure 41. 256-QAM performance for a Ricean fading channel for $\zeta = 2$.

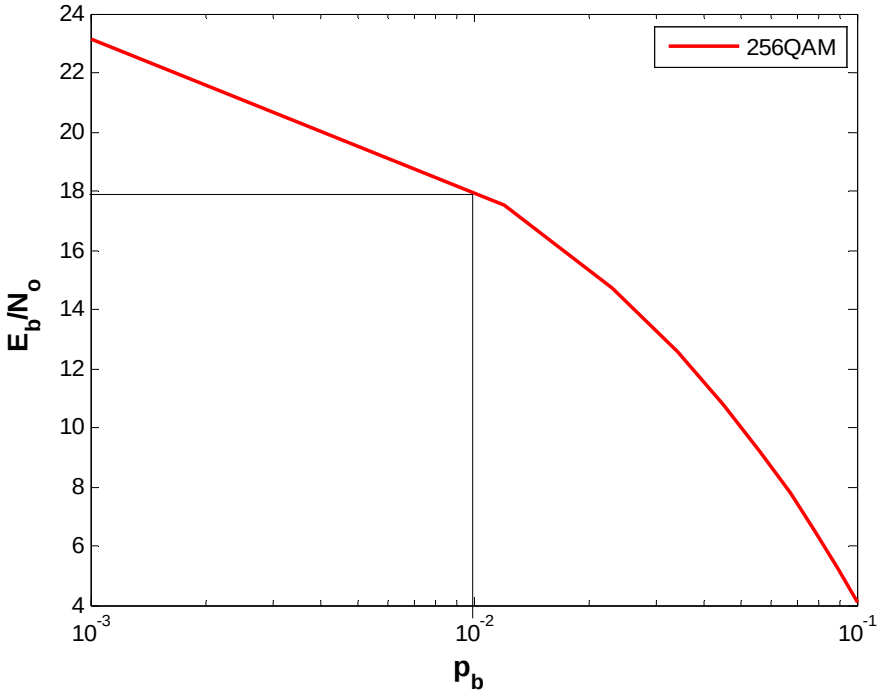

Figure 42. 256-QAM performance for a Ricean fading channel for $\zeta = 10$.

Odd numbered values of q were evaluated in the same manner by inverting Equation (5.14) for $\zeta = 2$ and $\zeta = 10$.

For 8-QAM and $\zeta = 2$, for a Ricean fading channel, we get

$$\gamma_b = \left[-3.7 \ln(p_b) - 10.7\sqrt{p_b} + 0.6 \right], \tag{5.21}$$

and

$$\gamma_b = \left[-1.2 \ln(p_b) - 16\sqrt{p_b} + 4.8 \right] \tag{5.22}$$

for 8-QAM and $\zeta = 10$.

Equations (5.21) and (5.22) are plotted in Figures 43 and 44, respectively. As can be seen, $E_b/N_o = 14\,\text{dB}$ and $E_b/N_o = 8.4\,\text{dB}$ are required to achieve $p_b = 10^{-2}$ when $\zeta = 2$ and 10, respectively.

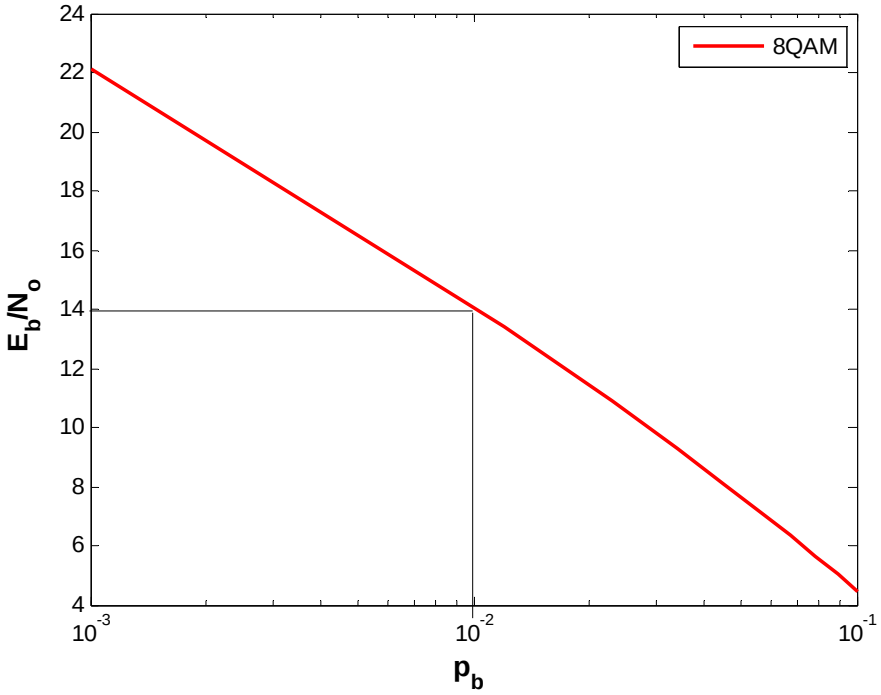

Figure 43. 8-QAM performance for a Ricean fading channel for $\zeta = 2$.

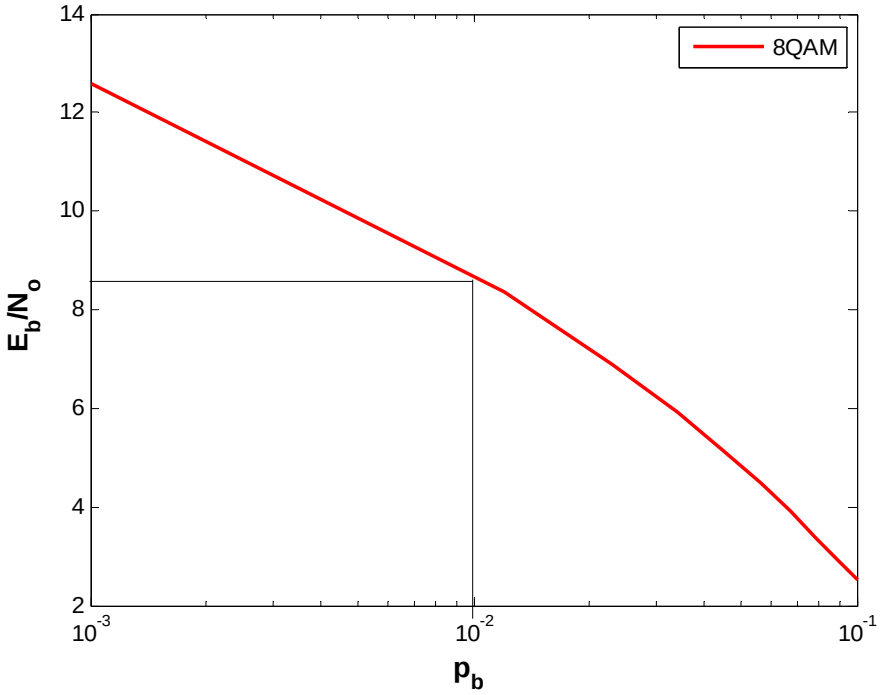

Figure 44. 8-QAM performance for a Ricean fading channel for $\zeta = 10$.

For 32-QAM and $\zeta = 2$, for a Ricean fading channel, we get

$$\gamma_b = \left[-0.6 \ln(p_b) - 41\sqrt{p_b} + 17 \right], \tag{5.23}$$

and

$$\gamma_b = \left[-0.12 \ln(p_b) - 41\sqrt{p_b} + 16.5 \right] \tag{5.24}$$

for 32-QAM and $\zeta = 10$.

Equations (5.23) and (5.24) are plotted in Figures 45 and 46, respectively. As can be seen, $E_b/N_o = 15.7$ dB and $E_b/N_o = 12.5$ dB are required to achieve $p_b = 10^{-2}$ when $\zeta = 2$ and 10, respectively.

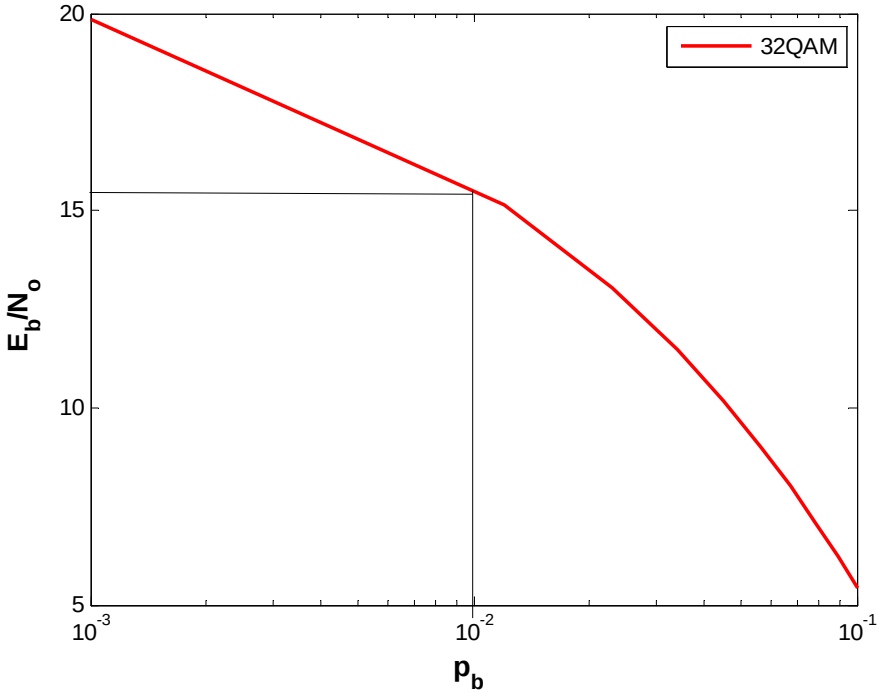

Figure 45. 32-QAM performance for a Ricean fading channel for $\zeta = 2$.

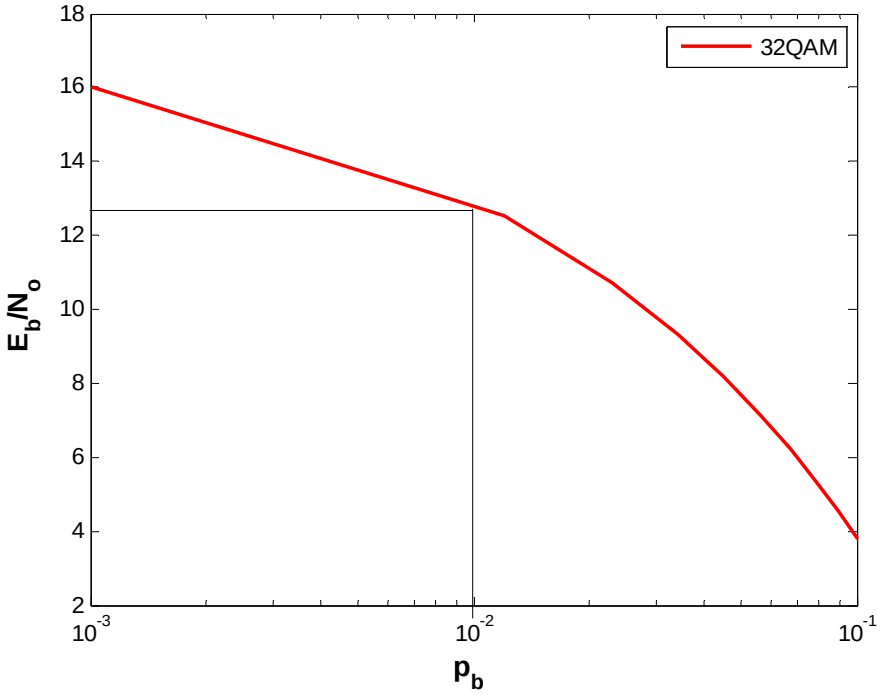

Figure 46. 32-QAM performance for a Ricean fading channel for $\zeta = 10$.

Although not typically used, 128-QAM was evaluated. For 128-QAM with $\zeta = 2$, we get

$$\gamma_b = \left[-1.7 \ln(p_b) - 45\sqrt{p_b} + 17 \right], \tag{5.25}$$

and

$$\gamma_b = \left[-0.9 \ln(p_b) - 42\sqrt{p_b} + 15.5 \right] \tag{5.26}$$

for 128-QAM and $\zeta = 10$.

Equations (5.25) and (5.26) are plotted in Figures 47 and 48, respectively. As can be seen, $E_b/N_o = 20$ dB and $E_b/N_o = 15.5$ dB, respectively, are required to achieve $p_b = 10^{-2}$ when $\zeta = 2$ and 10.

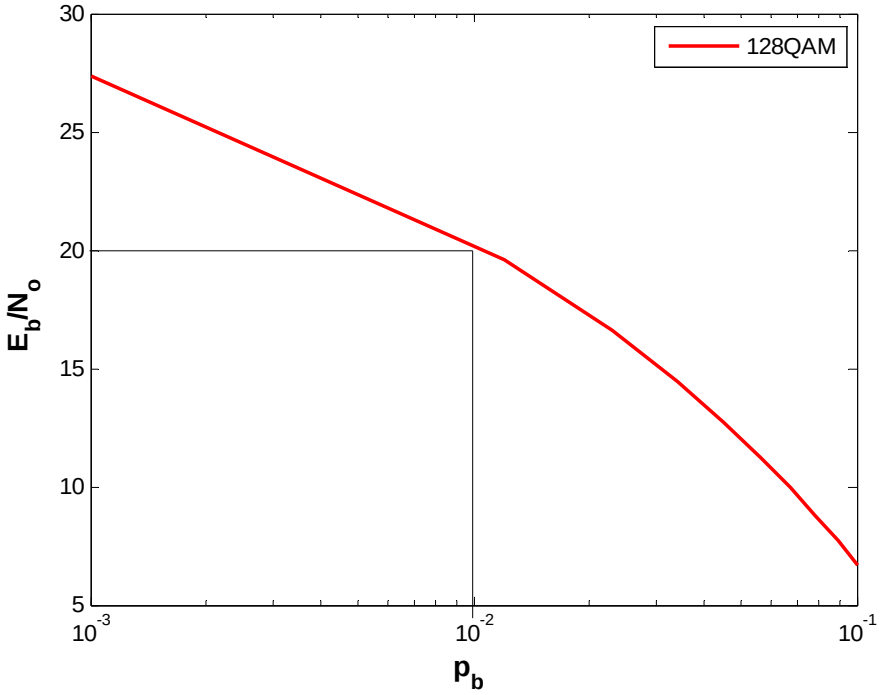

Figure 47. 128-QAM performance for a Ricean fading channel for $\zeta = 2$.

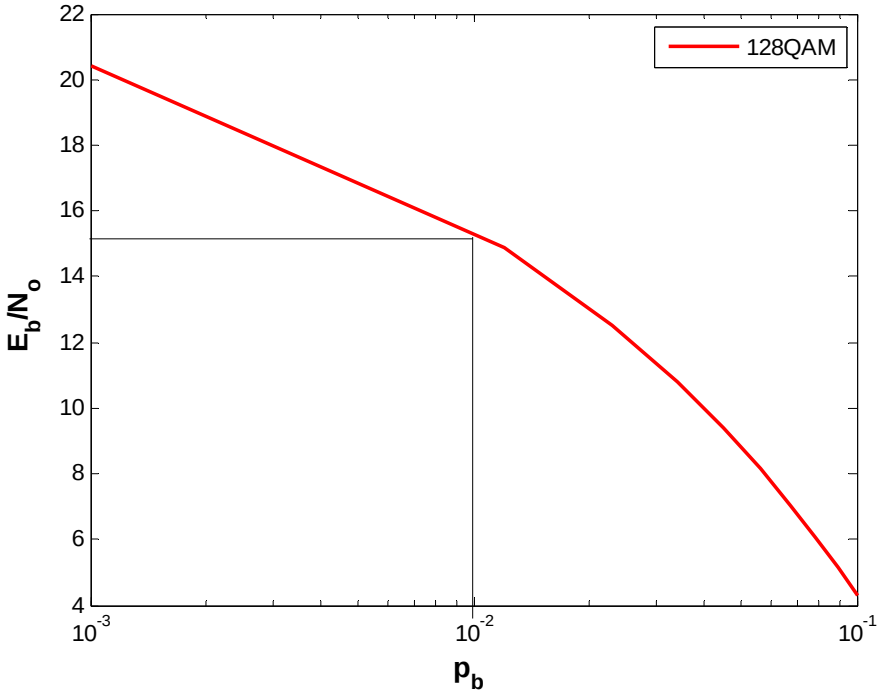

Figure 48. 128-QAM performance in Ricean fading channel for $\zeta = 10$.

4. GMSK

GMSK for a Ricean fading channel can be accurately modeled by [2]

$$p_b \approx \frac{1+\zeta}{2q\sqrt{\pi c}\left[1+\zeta+(q\delta\gamma_b)\right]}\exp\left[\frac{-(q\delta\zeta\gamma_b)}{\left(1+\zeta+(q\delta\gamma_b)\right)}\right]. \tag{5.27}$$

By applying logarithmic regression to Equation (5.27), we get

$$\gamma_b = \left[-3.7\ln(p_b) - 6.3\sqrt{p_b} - 3.8\right] \tag{5.28}$$

for GMSK and $\zeta = 2$ and

$$\gamma_b = \left[-1.3\ln(p_b) - 14\sqrt{p_b} + 3\right] \tag{5.29}$$

for GMSK and $\zeta = 10$.

Equations (5.28) and (5.29) are plotted in Figures 49 and 50, respectively. As can be seen, $E_b/N_o = 12.4\,\text{dB}$ and $E_b/N_o = 7.8\,\text{dB}$ are required to achieve $p_b = 10^{-2}$ when $\zeta = 2$ and 10.

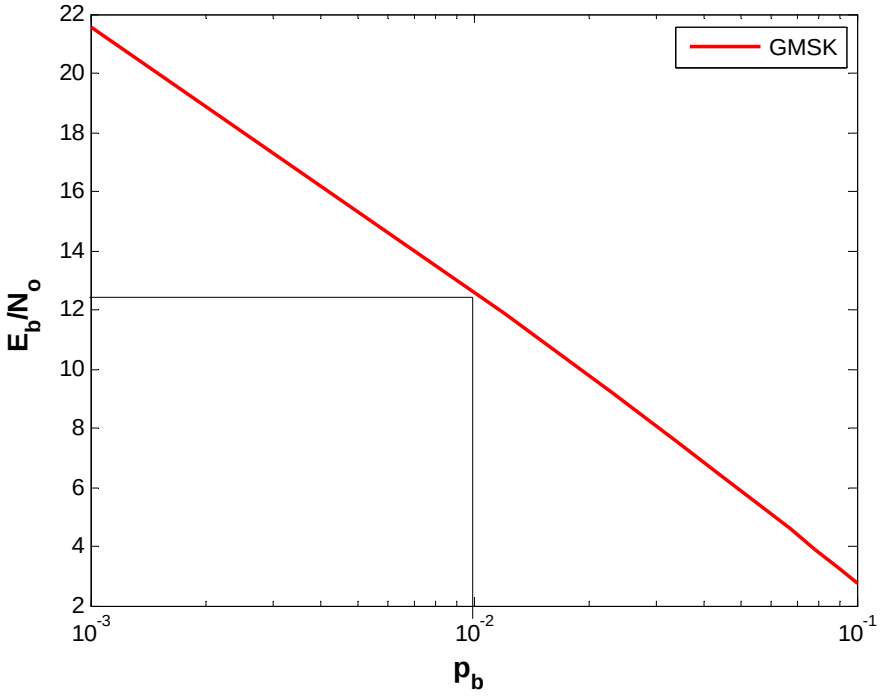

Figure 49. GMSK performance for a Ricean fading channel for $\zeta = 2$.

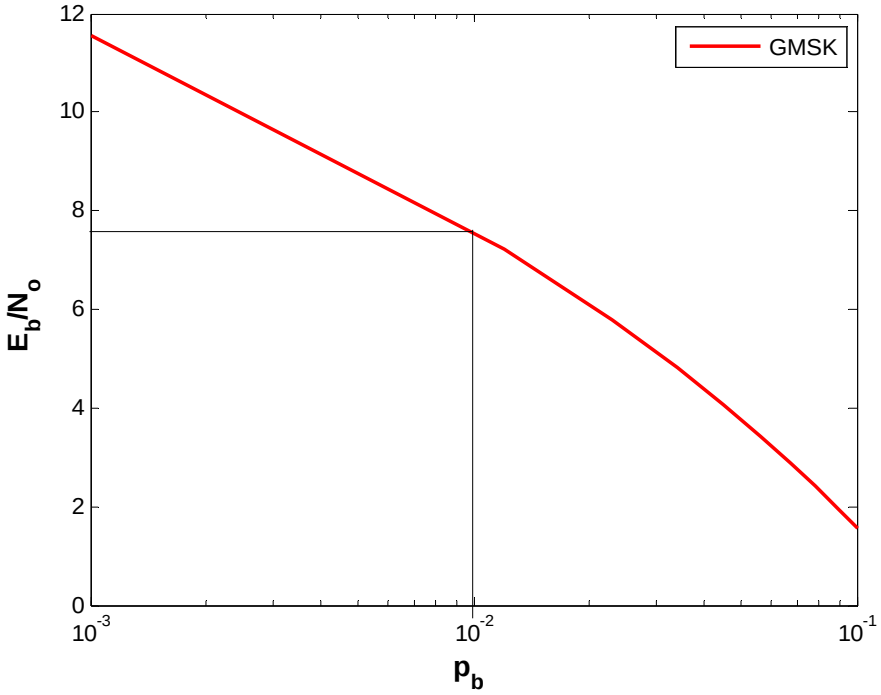

Figure 50. GMSK performance for a Ricean fading channel for $\zeta = 10$.

B. NONCOHERENT MODULATION, *M*-ARY ORTHOGONAL SIGNALING

Generic *M*FSK equations are good equation candidates for IMOM software. Specifically, 8-FSK, 16-FSK and 32-FSK are evaluated. For *M*FSK transmitted over a Ricean fading channel [2]

$$p_b = \frac{M}{2(M-1)} \sum_{n=1}^{M-1} \frac{(-1)^{n+1}(1+\zeta)}{1+\zeta+n(1+\zeta+q\gamma_b)} \binom{M-1}{n} \exp\left[\frac{-n\zeta q\gamma_b}{1+\zeta+n(1+\zeta+q\gamma_b)}\right]. \quad (5.30)$$

Using logarithmic regression, we invert Equation (5.30) to get

$$\gamma_b = \left[-4.3\ln(p_b) + 2.7\sqrt{p_b} - 6.3\right] \quad (5.31)$$

for 8-FSK and $\zeta = 2$ and

$$\gamma_b = \left[-1.6\ln(p_b) - 1.1\sqrt{p_b} - 0.338\right] \quad (5.32)$$

for 8-FSK and $\zeta = 10$.

Equations (5.31) and (5.32) are plotted in Figures 51 and 52, respectively. As can be seen, $E_b/N_o = 13.6\,\text{dB}$ and $E_b/N_o = 6.8\,\text{dB}$, respectively are required to achieve $p_b = 10^{-2}$ when $\zeta = 2$ and 10.

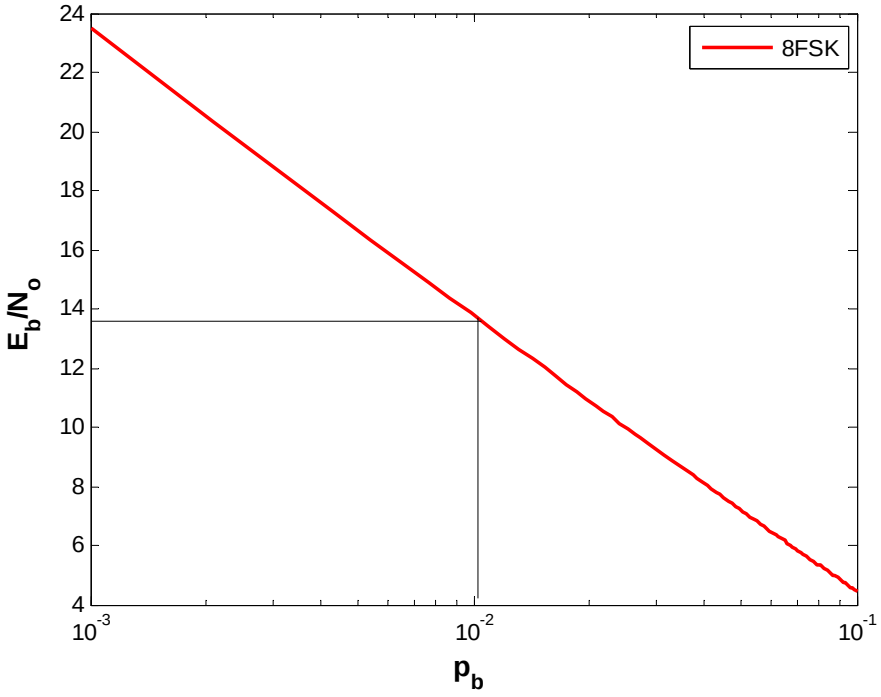

Figure 51. 8-FSK performance for a Ricean fading channel for $\zeta = 2$.

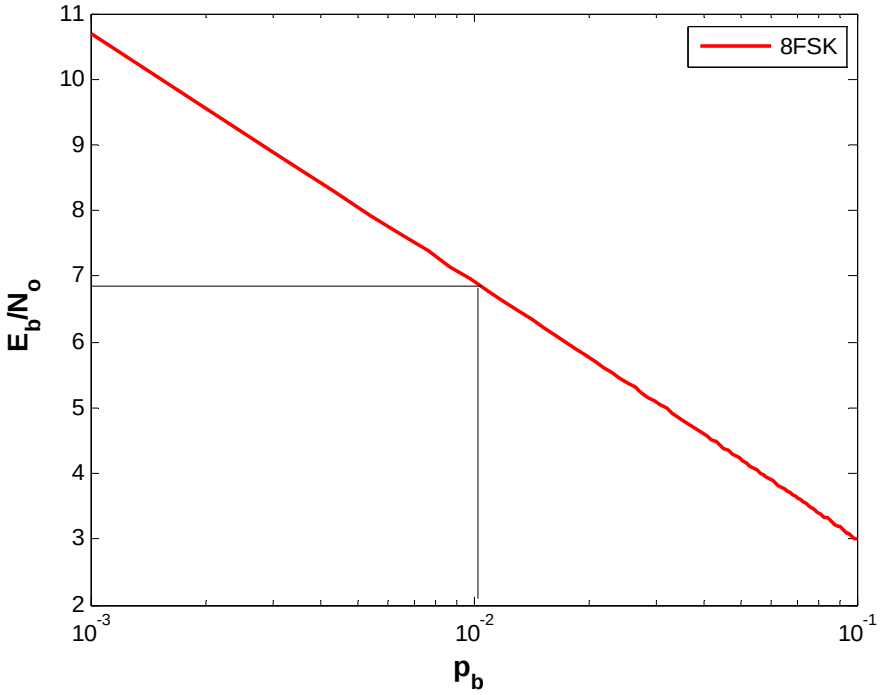

Figure 52. 8-FSK performance for a Ricean fading channel for $\zeta = 10$.

Similarly, from Equation (5.30),

$$\gamma_b = \left[-3.8 \ln(p_b) - 1.2\sqrt{p_b} - 4.6 \right] \tag{5.33}$$

for 16-FSK and $\zeta = 2$ and

$$\gamma_b = \left[-1.7 \ln(p_b) - 2.7\sqrt{p_b} - 1.9 \right] \tag{5.34}$$

for 16-FSK and $\zeta = 10$.

Equations (5.33) and (5.34) are plotted in Figures 53 and 54, respectively. As can be seen, $E_b/N_o = 13.3\,\text{dB}$ and $E_b/N_o = 6.1\,\text{dB}$, respectively, are required to achieve $p_b = 10^{-2}$ when $\zeta = 2$ and 10.

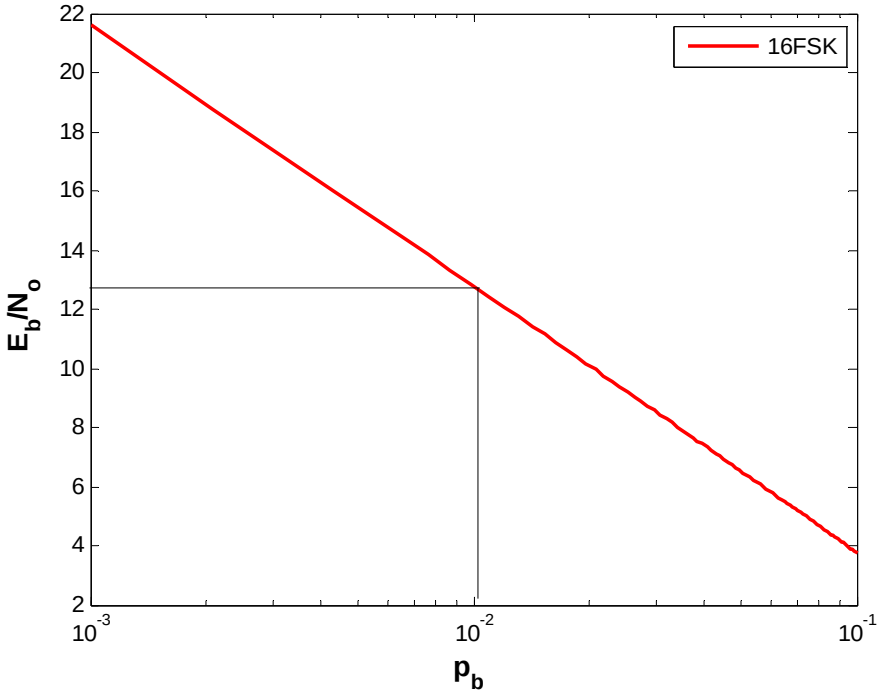

Figure 53. 16-FSK performance for a Ricean fading channel for $\zeta = 2$.

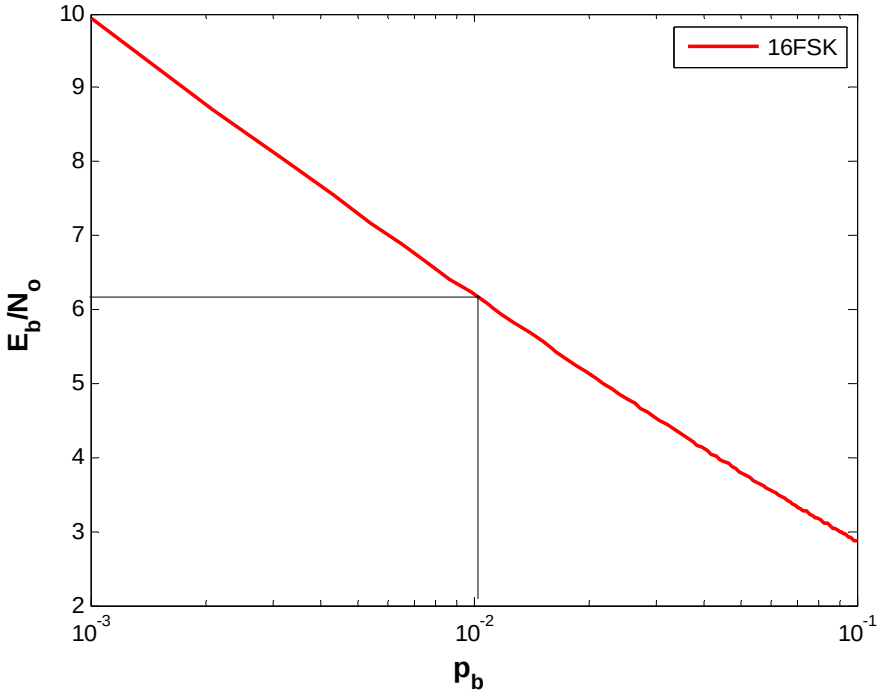

Figure 54. 16-FSK performance for a Ricean fading channel for $\zeta = 10$.

For 32-FSK and Ricean fading with $\zeta = 2$, we get

$$\gamma_b = \left[-3.9 \ln(p_b) - 0.4\sqrt{p_b} - 5.1 \right], \tag{5.35}$$

and

$$\gamma_b = \left[-1.8 \ln(p_b) + 5.6\sqrt{p_b} - 3.1 \right] \tag{5.36}$$

for 32-FSK and $\zeta = 10$.

Equations (5.35) and (5.36) are plotted in Figures 55 and 56, respectively. As can be seen, $E_b/N_o = 12.6\,\text{dB}$ and $E_b/N_o = 5.6\,\text{dB}$, respectively, are required to achieve $p_b = 10^{-2}$ when $\zeta = 2$ and 10.

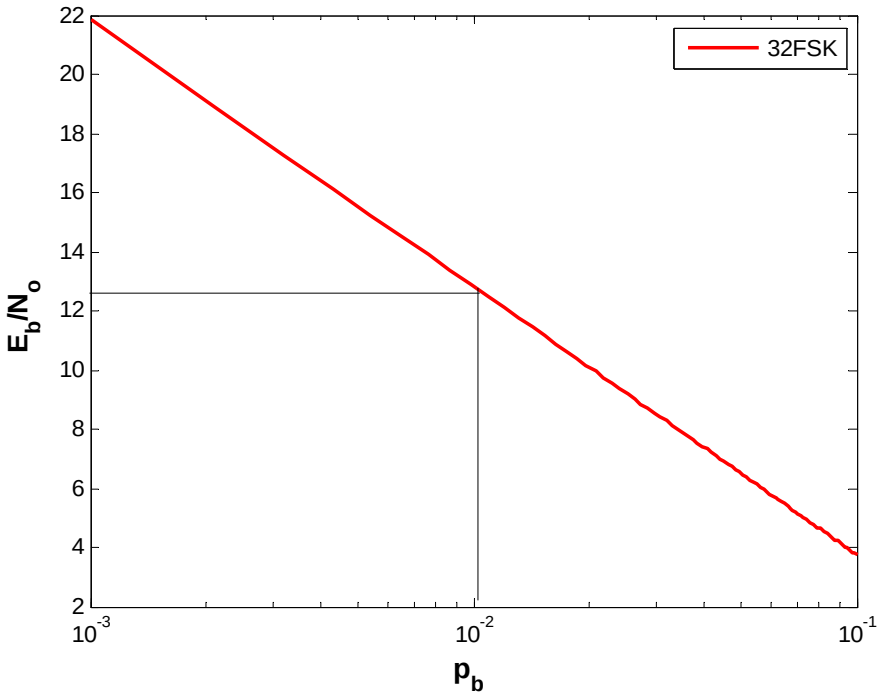

Figure 55. 32-FSK performance in Ricean fading channel for $\zeta = 2$.

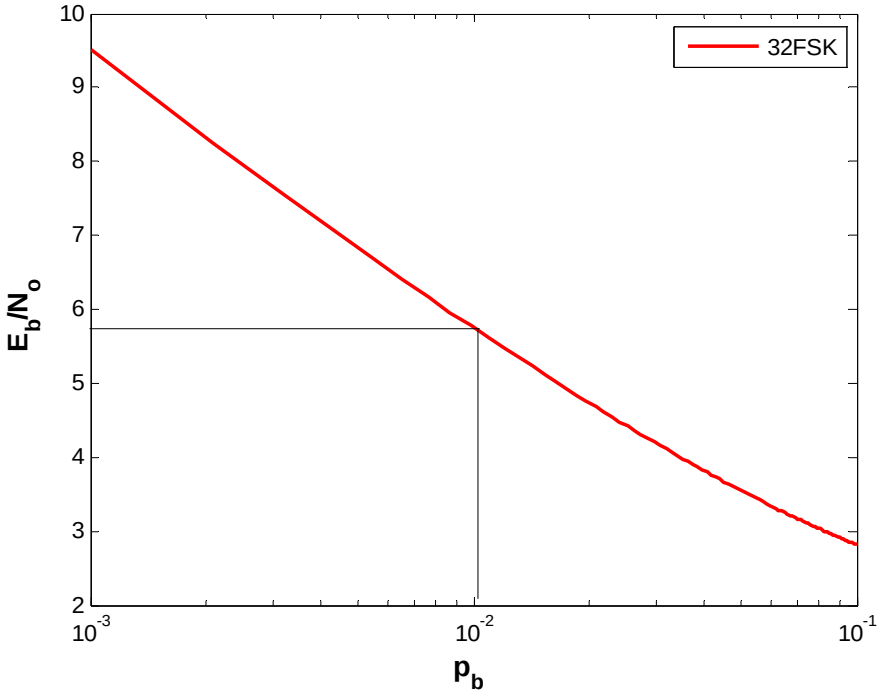

Figure 56. 32-FSK performance for a Ricean fading channel for $\zeta = 10$.

Expressions for the signal-to-noise ratio as functions of the probability of channel bit error for Ricean fading channels were developed in this chapter. The next chapter extends the methodology to a specific system, the Joint Tactical Information Distribution System (JTIDS).

VI. JOINT TACTICAL INFORMATION DISTRIBUTION SYSTEM

JTIDS is used by the U.S. Armed Forces and its allies to support data communications needs. JTIDS serves many purposes. Various platforms are supported by JTIDS as seen in Figure 57. Equation Chapter (Next) Section 6

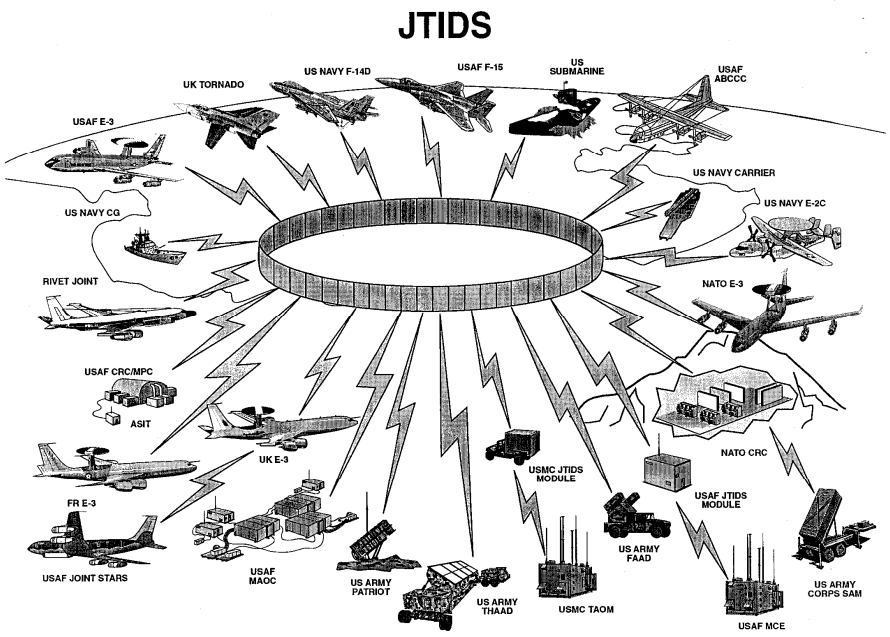

Figure 57. General overview of JTIDS applications [5].

JTIDS is a complex system with different transmission modes, but, for this thesis only the single-pulse architecture is evaluated. The single-pulse architecture sacrifices security and jam resistance for an increased data rate. JTIDS uses (31, 15) Reed Solomon (RS) coding, providing secure, jam resistant, digital data communication [7]. The modulation technique used in JTIDS is cyclical code-shift keying (CCSK). When system specifics are known, a more accurate result can be obtained than with the generic procedure developed in the preceding chapters.

The probability of channel symbol error for the JTIDS single-pulse architecture is [7]

$$p_s = \sum_{j=0}^{32} \zeta_j \binom{32}{j} p_c^j (1-p_c)^{32-j} \tag{6.1}$$

where the $\zeta_j s$ are given in Table 2 and p_c is the probability of chip error. For noncoherent detection:

$$p_c = \left(\frac{1}{2}\right) e^{-5\gamma_b/32}. \tag{6.2}$$

For the (31,15) RS code used in JTIDS, the probability of information bit error is given by [7]

$$P_b \approx \frac{0.6}{31} \sum_{i=9}^{31} i \binom{31}{i} p_s^i (1-p_s)^{31-i} \tag{6.3}$$

which is plotted in Figure 58. From Figure 58, we see that $p_s = 0.058$ is required to achieve $P_b = 10^{-5}$. Note that knowledge of the specific error correction coding used allows us to obtain a JTIDS-specific result instead of a generic result as in previous chapters.

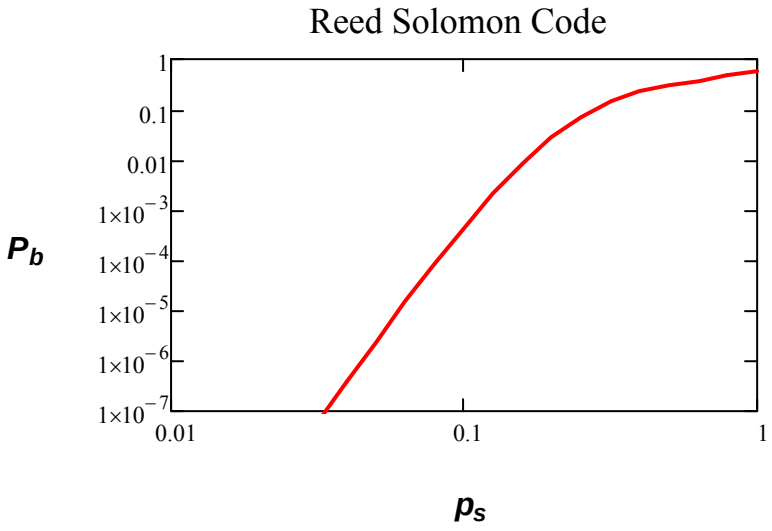

Figure 58. JTIDS probability of info bit error vs. probability of channel symbol error.

Table 2. Conditional probabilities of channel symbol error ζ_j for JTIDS [7].

j	ζ_j
0	0
1	0
2	0
3	0
4	0
5	0
6	0
7	0.0015
8	0.0221
9	0.1126
10	0.3669
11	0.7093
12	0.9351
…	1.0
32	1.0

Substituting Equation (6.2) into (6.1) and using the logarithmic regression curve fitting technique, we get

$$\gamma_b = \left[-0.207 \ln(p_s) - 6.2\sqrt{p_s} + 9 \right] \tag{6.4}$$

which is plotted in Figure 59. From Figure 59, we see that $E_b/N_o = 8.1\,\text{dB}$ is required to obtain $p_b = 0.058$, which implies an information bit error of $P_b = 10^{-5}$.

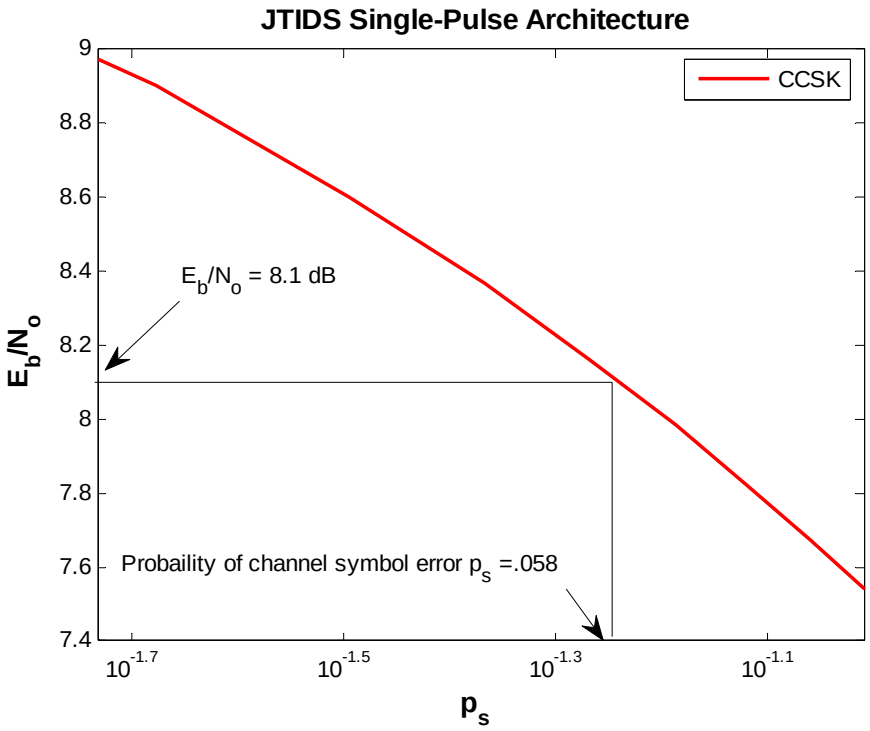

Figure 59. JTIDS performance as a function of probability of channel symbol error.

In this chapter, unlike previous chapters, performance specific to JTIDS was examined. In the final chapter, conclusions and recommendations for future work are discussed.

VII. CONCLUSIONS AND FUTURE WORK

A. CONCLUSIONS

A methodology that can be incorporated into the IMOM software suite was developed in this thesis. Currently, IMOM does not take the effect of multipath small scale fading or digital communications into account in its evaluation of the link budget equation. The intent of this thesis was to develop results for various common digital modulation schemes that could be implemented in IMOM regardless of the FEC coding scheme. Due to the ever changing communications environment and advancements in communications technology, it is important for IMOM to remain flexible. The key to ensuring compatibility with IMOM was to obtain analytic expressions for required signal-to-noise ratio as a function of probability of channel bit error in lieu of the more traditional expressions for probability of channel bit error in terms of signal-to-noise ratio.

The results obtained in this thesis will ultimately be used in the link budget analysis equation to give users of IMOM a greater sense of situational awareness when interpreting data provided by the software. The modulation techniques evaluated are generic and yet are intended to give a baseline for more specific applications that this method could ultimately provide. Many of the commonly used digital modulation techniques for wireless communications and military applications were evaluated in this thesis. While some approximations were used, they are extremely accurate over the operating range associated with most systems. However, should specific requirements change; the equations could easily be altered to apply to modified operating ranges.

The results obtained were generic in nature to allow flexibility and fluidity when insufficient information is known. As specific system driven applications arise and the number of digital modulation schemes increases, the accuracy of IMOM is significantly improved by allowing for the specific modulation type. More importantly, IMOM must adapt to an increase in digital communications systems, which it currently does not. It is also important to note that the results assume forward error correction coding, which is a

safe assumption for digital communications. However, code types and whether soft or hard decision decoding is used are factors not fully explored in this thesis except for JTIDS.

Non-fading, Rayleigh and Ricean fading channels were each addressed for the more common modulation techniques. These represent models for digital communications channels that encompass a significant portion of multipath fading. In essence, they span the spectrum from complete line-of-sight to no line-of-sight or a mixture of the two. As expected, as the line-of-sight signal component decreased, the required signal-to-noise ratio increased.

Logarithmic regression curve fitting was an instrumental tool in deriving many of the inverted equations. This technique was important for inverting equations that could not be inverted analytically. The inverted equations were optimized for $p_b = 10^{-2}$, which translates to a probability of data or information bit error on the order of magnitude of $P_b = 10^{-5}$. This value is in line with what is specified by many wireless communications standards. However, should other values be required, the expressions can be optimized accordingly.

Ricean fading channels introduced the biggest variance into the inverted equations. This was due primarily to the introduction of the direct-to-diffuse signal power parameter ζ. We were able to mathematically obtain results for $\zeta \le 12$, however, for $\zeta > 12$, numerical problems prevented a successful inversion. It can be inferred that this is due to the fact that for $\zeta > 12$ the channel should be modeled as a non-fading channel.

The results obtained for each of the modulation techniques considered in this thesis for several multipath fading channels are summarized in Tables 3-6.

Table 3. E_b/N_o for modulation techniques and a non-fading channel for $p_b = 10^{-2}$.

BPSK/QPSK	***4.3 dB***
8-PSK	***9.7 dB***
16-PSK	***15.5 dB***
16-QAM	***7.8 dB***
64-QAM	***11.8 dB***
256-QAM	***16.2 dB***
8-QAM	***6.7 dB***
32-QAM	***10 dB***
128-QAM	***14.1 dB***
GMSK	***5.7 dB***
8-FSK	***5.5 dB***
16-FSK	***4.7 dB***
32-FSK	***4.3 dB***

Table 4. E_b/N_o for modulation techniques and a Rayleigh fading channel for $p_b = 10^{-2}$.

BPSK/QPSK	***14.4 dB***
8-PSK	***15 dB***
16-PSK	***18.6 dB***
16-QAM	***9.5 dB***
64-QAM	***16.5 dB***
256-QAM	***29 dB***
8-QAM	***17 dB***
32-QAM	***19 dB***
128-QAM	***21 dB***
GMSK	***15.4 dB***
8-FSK	***16.7 dB***
16-FSK	***16.3 dB***
32-FSK	***15.8 dB***

Table 5. E_b/N_o for modulation techniques and a Ricean fading channel for $p_b = 10^{-2}$ with $\zeta = 2$.

BPSK/QPSK	***11 dB***
8-PSK	***13.3 dB***
16-PSK	***16.8 dB***
16-QAM	***13 dB***
64-QAM	***17 dB***
256-QAM	***22 dB***
8-QAM	***14 dB***
32-QAM	***15.7 dB***
128-QAM	***20 dB***
GMSK	***12.4 dB***
8-FSK	***13.6 dB***
16-FSK	***13.3 dB***
32-FSK	***12.6 dB***

Table 6. E_b/N_o for modulation techniques and a Ricean fading channel for $p_b = 10^{-2}$ with $\zeta = 10$.

BPSK/QPSK	***5.8 dB***
8-PSK	***8.8 dB***
16-PSK	***12 dB***
16-QAM	***6 dB***
64-QAM	***13.5 dB***
256-QAM	***18 dB***
8-QAM	***8.4 dB***
32-QAM	***12.5 dB***
128-QAM	***15.5 dB***
GMSK	***7.8 dB***
8-FSK	***6.8 dB***
16-FSK	***6.1 dB***
32-FSK	***5.6 dB***

B. FUTURE RESEARCH AREAS

We have examined the impact that incorporating the effect of specific digital modulation techniques into IMOM can have on improving the accuracy in evaluating the link budget analysis equation. Multipath fading is important, yet not currently implemented in the current version of IMOM.

An important concept that was mentioned, yet not evaluated, is the double-pulse architecture of the JTIDS. This architecture is much more complicated, yet provides additional levels of security at the expense of decreased data rate. Evaluating the double-pulse structure of JTIDS would enhance the capability of IMOM even further.

IMOM could also profit from the evaluation of additional specific digital modulation systems in the same manner that JTIDS was evaluated. Based on user needs, a development of specific systems could be implemented and incorporated into a data bank which operators could use to improve the accuracy of IMOM.

THIS PAGE INTENTIONALLY LEFT BLANK

LIST OF REFERENCES

[1] B. Sklar, *Digital Communications, Fundamentals and Applications, 2nd ed.,* Prentice Hall PTR, Upper Saddle River, NJ, 1995.

[2] R. Clark Robertson and Nathan E. Beltz, *Digital Communications Over Fading Channels*, Naval Postgraduate School, Monterey, CA, Nov 2004.

[3] J. G. Proakis, *Digital Communications, 4th ed*., McGraw-Hill, New York, NY, 2001.

[4] Clark Robertson, *Notes for EC4550 Digital Communications*, Naval Postgraduate School, Monterey, CA, 2007.

[5] Commanding Officer Navy Center for Tactical Systems Interoperability (NCTSI), *Understanding Link-16; A Guidebook for New Users*, Northrop Grumman Corporation, San Diego, CA, 2001.

[6] T. S. Rappaport, *Wireless Communications, principles and practices, 2nd ed.*, Prentice Hall PTR, Upper Saddle River, NJ, 2002.

[7] Chi-Han Kao, Clark Robertson, and Kyle Lin, *Performance Analysis and Simulation of Cyclic Code-Shift Keying*, to be published in *Proc. of IEEE Military Communications Conference*, 2008.

THIS PAGE INTENTIONALLY LEFT BLANK

INITIAL DISTRIBUTION LIST

1. Defense Technical Information Center
   Ft. Belvoir, Virginia

2. Dudley Knox Library
   Naval Postgraduate School
   Monterey, California

3. Chairman, Code EC
   Department of Electrical and Computer Engineering
   Naval Postgraduate School
   Monterey, California

4. Professor R. Clark Robertson, Code EC/Rc
   Department of Electrical and Computer Engineering
   Naval Postgraduate School
   Monterey, California

5. Assistant Professor Frank Kragh, Code EC/Kh
   Department of Electrical and Computer Engineering
   Naval Postgraduate School
   Monterey, California

6. Captain Jose H. Hernandez Jr.
   Department of Electrical and Computer Engineering
   Naval Postgraduate School
   Monterey, California

7. First Lieutenant Ryan Hemperly
   USAF 453rd Electronic Warfare Squadron
   U.S. Air Force
   San Antonio, Texas

8. Lothar Deil
   USAF 453rd Electronic Warfare Squadron
   U.S. Air Force
   San Antonio, Texas

9. Kurt D. Welker
   Idaho National Laboratory
   Battelle Energy Alliance. LLC
   Idaho Falls, Idaho